



HAL
open science

Assessing satellite-derived fire patches with functional diversity trait methods

M. Vanesa Moreno, Pierre Laurent, Philippe Ciais, Florent Mouillot

► To cite this version:

M. Vanesa Moreno, Pierre Laurent, Philippe Ciais, Florent Mouillot. Assessing satellite-derived fire patches with functional diversity trait methods. *Remote Sensing of Environment*, 2020, 247, 10.1016/j.rse.2020.111897 . hal-02844066

HAL Id: hal-02844066

<https://hal.science/hal-02844066>

Submitted on 3 Jun 2022

HAL is a multi-disciplinary open access archive for the deposit and dissemination of scientific research documents, whether they are published or not. The documents may come from teaching and research institutions in France or abroad, or from public or private research centers.

L'archive ouverte pluridisciplinaire **HAL**, est destinée au dépôt et à la diffusion de documents scientifiques de niveau recherche, publiés ou non, émanant des établissements d'enseignement et de recherche français ou étrangers, des laboratoires publics ou privés.



Distributed under a Creative Commons Attribution - NonCommercial 4.0 International License

1 **A new trait-based method to evaluate satellite-derived fire-patch morphology**

2 M. Vanesa MORENO a, *, Pierre LAURENT b, Philippe CIAIS b, Florent MOUILLOT a

3 a UMR CEFE 5175, Centre National de la Recherche Scientifique, Université de Montpellier,
4 Université Paul-Valéry Montpellier, Ecole Pratique des Hautes Etudes, Institut de Recherche
5 pour le Développement, 1919 route de Mende, 34293 Montpellier CEDEX 5, France

6 b Laboratoire des Sciences du Climat et de l'Environnement, CEA-CNRS-UVSQ, UMR8212,
7 Gif-sur-Yvette, France

8 * Corresponding author.

9 UMR CEFE 5175, Centre National de la Recherche Scientifique, Université de Montpellier,
10 Université Paul-Valéry Montpellier, Ecole Pratique des Hautes Etudes, Institut de Recherche
11 pour le Développement, 1919 route de Mende, 34293 Montpellier CEDEX 5, France

12 E-mail address: vanesa.moreno@cefe.cnrs.fr (M.V. Moreno).

13

14

15

16

17

18

19

20

21

22

23

24 **Abstract**

25 Fire disturbance is a significant component of the climate system. Analysis of satellite-
26 derived burned areas has allowed the identification of fire patches and their morphology as a
27 new resource for tracking fire spread to improve fire models used to assess the impact of
28 fires on climate and the carbon cycle. A critical parameter of the flood-fill algorithm used to
29 create fire patches is the cut-off (in days) below which it aggregates two contiguous burned
30 pixels to the same fire patch. However, the current level of validation is insufficient to
31 understand the effect of the cut-off values and sensor resolutions on the subsequent fire-
32 patch morphology. The FRY v1.0 database of functional fire-patch traits (e.g., size,
33 elongation, and direction) emanates from the analyses of two global burned-area products
34 derived from MODIS and MERIS sensors with different spatial and temporal resolutions and
35 with cut-off values of 3, 5, 9, and 14 days. To evaluate whether the FRY products are
36 conserving the spatial features of fire patches and what are the most realistic cut-off values
37 to use in different sub-regions of North America, we propose a new functional diversity trait-
38 based approach, which compares the satellite-derived fire patches to forest service
39 perimeters as reference data. This paper shows the accuracy of the FRY fire patches ≥ 300
40 ha in North America during 2005–2011. Our analysis demonstrates that fire patches with a
41 high cut-off of 14 days and those derived from MODIS sensors, with their high temporal
42 resolution, better conserve the fire diversity in North America. In conclusion, our statistical
43 framework can be used for assessing satellite-derived fire patches. Furthermore, the
44 temporal resolution of satellite sensors is the most important factor in identifying fire patches
45 — thus space agencies should consider it when planning the future development of cost-
46 effective climate observation systems.

47 **1. Introduction**

48 Fire is the source of approximately one third of aerosol, greenhouse gas and other trace gas
49 emissions. This biomass burning leads to major effects on the abundance and diversity of

50 vegetation, carbon and water cycling, and as a result, the overall climate system (Andreae,
51 2019; Andreae and Merlet, 2001; Bowman et al., 2009; van der Werf et al., 2010). Spatial
52 and temporal monitoring of fire disturbances is thus essential to benchmark the fire models
53 used to assess fire-climate feedbacks and the impact of fires on climate and the carbon
54 cycle. Indeed, fire disturbance is one of the Essential Climate Variables (ECVs) that is listed
55 by the Global Climate Observation System (GCOS) as a critical component in the climate
56 system (WMO, 2016).

57 Out of the different satellite-derived fire disturbance products, burned areas are the most
58 commonly used for the development and evaluation of fire modules embedded in Dynamic
59 Global Vegetation Models (DGVMs) (Bistinas et al., 2014; Hantson et al., 2016; Mouillot et
60 al., 2014). However, burned-area products alone do not allow a process-oriented
61 development of fire modules. For instance, a bias of ignition numbers can compensate a
62 bias of fire size in a model, and still match observed burned area (e.g., Yue et al., 2014).
63 One critical aspect of fire modules not yet evaluated on a systematic basis is how they
64 simulate the spread of fires. Many models simulate fire spread based on Rothermel's
65 equation (Rothermel, 1972). This equation assumes that fires form an ellipse of burned area
66 centred on each ignition point — it assumes homogeneous vegetation and topography, and
67 a constant wind direction (Rabin et al., 2017).

68 Fire-patch products have emerged from pixel-level burned-area products. These fire-patch
69 products work on the principle that contiguous burned pixels occurring during the same
70 period of time can be aggregated into a single patch. The critical parameter in those
71 algorithms is called the cut-off (in days), defined as the maximum time period below which
72 consecutive neighbouring burned pixels can be grouped into the same patch. For example,
73 at the continental or local scale, Archibald and Roy (2009), and Nogueira et al. (2017) used
74 a cut-off of 8 days in Africa and central Brazil respectively, while Fusco et al. (2019) used a
75 cut-off of 9 days in the United States. At the global scale, Hantson et al. (2015) used a cut-
76 off of 14 days, while Laurent et al. (2018a) tested cut-offs of 3, 5, 9, and 14 days to produce

77 the global FRY v1.0 fire-patch functional traits database. A source of uncertainty in the
78 determination of the cut-off parameter arises from the fact that burned areas derived from
79 low Earth orbit satellite observations are not continuous in time. For example, the presence
80 of clouds may mask burned-area pixels that occur between two consecutive observations
81 with clear-sky conditions as implemented in new algorithms accounting for uncertainty in the
82 date-of-burning (Andela et al., 2019; Campagnolo et al., 2019; Oom et al., 2016).
83 Geostationary satellites might be better, but they are still affected by persistent clouds. The
84 arbitrary choice of a cut-off value in fire-patch products and the current lack of assessment
85 of their uncertainties (Boschetti et al., 2019; Padilla et al., 2014) hinders the use of these
86 products for quantitative evaluation of fire models.

87 Assessment of uncertainties in satellite-derived ECVs is essential if they are to be used
88 effectively in climate modelling (WMO, 2016). Two assessments (validation and
89 intercomparison) are required by GCOS: where validation is the process of assessing the
90 accuracy of satellite-derived products using independent reference data (Boschetti et al.,
91 2006). Based on the GCOS scientific and technical requirements, the Land Product
92 Validation (LPV) subgroup of the Committee on Earth Observation Satellites (CEOS)
93 Working Group on Calibration and Validation (WGCV) is developing protocols for the
94 assessment of uncertainties in products based on satellite observations at five different
95 validation stages (Boschetti and Justice, 2009). Considerable effort has been put into the
96 validation of moderate spatial resolution burned-area products at the global scale, reaching
97 CEOS validation stage 3 (Padilla et al., 2014). The validation relies on the acknowledged
98 cross-tabulation approach of quantifying omission and commission errors in addition to the
99 overall accuracy using high-resolution imagery as reference data. (Boschetti et al., 2006).
100 However, the evaluation does not cover fire-patch morphology, which is needed to model
101 fire spread processes. Fire spread can be subject greater error than is found in burned area,
102 because pixels may be wrongly committed or omitted particularly at the fire-patch edge
103 (Humber et al., 2019).

104 At the local scale, in central Brazil, Nogueira et al. (2017) assessed overlapping fire patches
105 using high-resolution Landsat imagery as reference data and estimated patch-to-patch
106 correlations of their morphological features. In a similar approach, Chuvieco et al. (2018,
107 2016) used forest service perimeters, while Andela et al. (2019) used high-resolution
108 imagery and fire duration by combining perimeters of fire patches using VIIRS active fire
109 detection. Fusco et al. (2019) assessed the positive and negative rates of detection between
110 fire patches and forest service reports in the United States. In this study, we propose an
111 original statistical framework for fire ecology, to probe the spatial conservation of fire-patch
112 morphology across sensors.

113 We evaluated the fire-patch functional traits products provided in the global FRY v1.0
114 database described by Laurent et al. (2018a). This database allows series of data to be
115 calculated with different cut-offs of 3, 6, 9, and 14 days from two global burned-area
116 products: MERIS Fire_cci version 4.1 (FireCCI41; Chuvieco et al., 2016) and MODIS
117 MCD64A1 collection 6 (MCD64A1; Giglio et al., 2018). The MERIS and MODIS sensors
118 have different temporal (~1 day with MODIS to 3 days with MERIS) and spatial (~300 m with
119 MERIS to 500 m with MODIS) resolutions. These contrasting temporal and spatial
120 resolutions allowed us to examine whether a higher temporal resolution or a higher spatial
121 resolution leads to the best evaluation performance, and to specify future requests for new
122 global burned-area developments. This issue is still open because Laurent et al. (2018a)
123 performed only an intercomparison between the two sensors — i.e., they performed a CEOS
124 validation stage 0, but no evaluation.

125 To assess whether the FRY products (Laurent et al., 2018a) provide realistic fire-patch traits,
126 we applied a new functional diversity trait-based approach widely used in species
127 assemblage comparative studies (Mouillot et al., 2013; Villéger et al., 2013, 2008). The
128 approach compares the functional space built on morphological traits of individual fire
129 patches, of assemblages of fire patches ≥ 300 ha from the two FRY products with cut-offs of
130 3, 5, 9, and 14 days to reference data derived from forest service perimeters (Canadian

131 Forest Service, 2014; U.S. Geological Survey, 2017) in North America during the period
132 2005–2011. This method is now considered as a statistical reference framework in
133 community ecology; we tested its efficiency when applied to fire-patch assemblages defined
134 by their morphological traits. We examined whether the FRY-FireCCI41 product based on
135 the MERIS sensor with a lower temporal resolution and a higher spatial resolution is better
136 or worse than the FRY-MCD64A1 based on the MODIS sensor regarding fire-patch
137 diversity; and what are the most realistic cut-off parameter values to use in different sub-
138 regions of North America.

139 **2. Methods**

140 *2.1. Data*

141 *2.1.1. FRY v1.0 database*

142 FRY is a global database of fire patches, defined by their morphological features, also
143 known as their functional traits. These features are established from two satellite-derived
144 pixel-level burned-area products and computed with four cut-off values (Laurent et al.,
145 2018a, 2018b). The two FRY products correspond to the processing of global burned-area
146 products from FireCCI41 and MCD64A1. Both burned-area products overlapped during the
147 2005–2011 time period. MCD64A1 (Giglio et al., 2018) is based on the MODIS sensor
148 aboard the Terra and Aqua satellites, with a spatial resolution of 500 m and a temporal
149 resolution of one day. It was created by hybrid algorithms that combine thermal information
150 from the MODIS MCD14A1 collection 6 active fire product (Giglio et al., 2016) and post-fire
151 reflectance. FireCCI41 (Chuvieco et al., 2016) uses the post-fire reflectance from the MERIS
152 sensor, aboard the Envisat satellite with a spatial resolution of 300 m at nadir and a temporal
153 resolution of three days.

154 The flood-fill algorithm used to determine the FRY patches aggregates neighbouring burned
155 pixels with differences in the date-of-burning below a given time threshold, defined as cut-off
156 values of 3, 5, 9, and 14 days. If the time elapsed between the date-of-burning of two

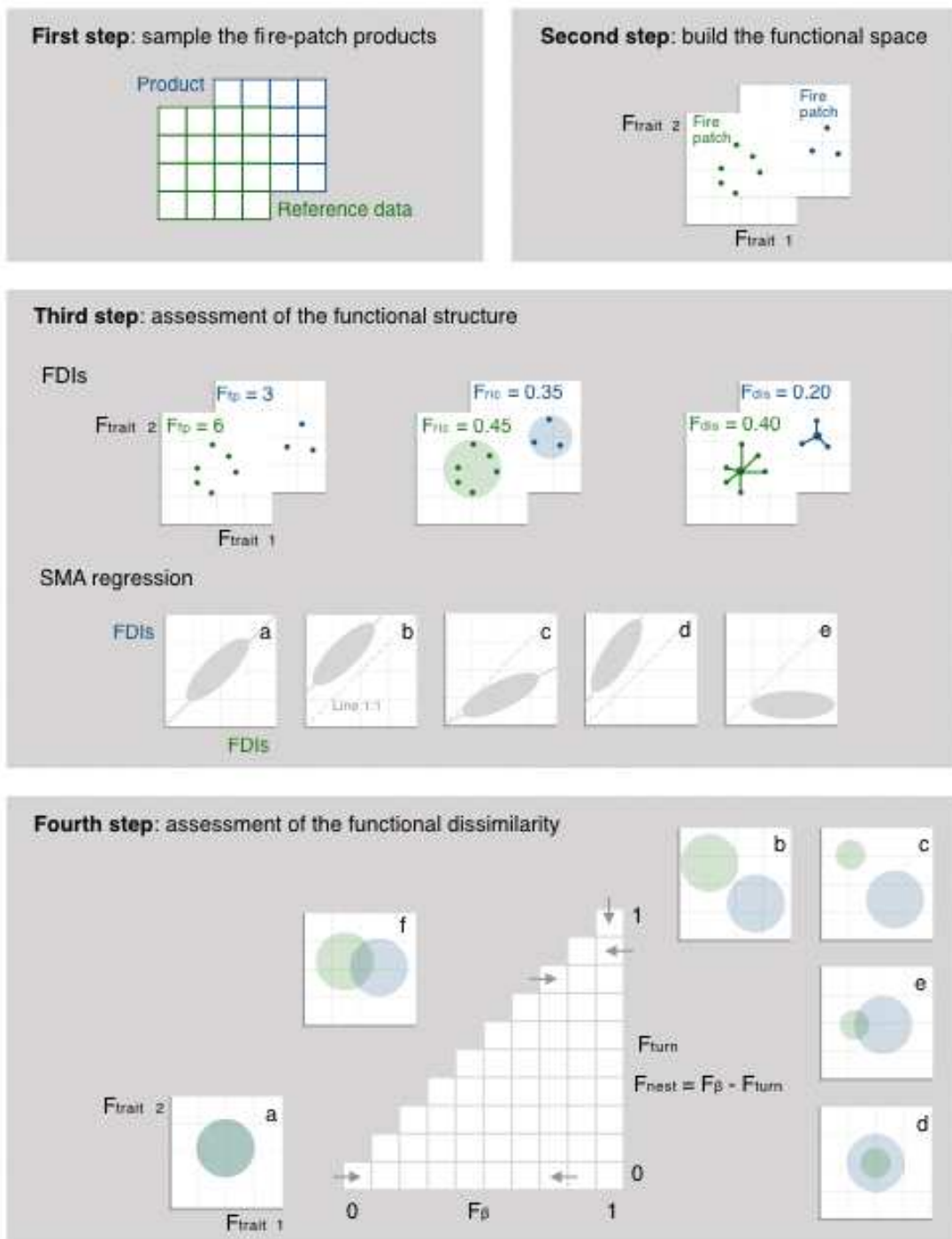
157 neighbouring pixels exceeds the cutoff value, a new fire patch is created (Laurent et al.,
158 2018a). FRY also aims to provide functional fire-patch traits as morphological descriptors
159 relevant to the underlying spreading processes (Laurent et al., 2018a). For example, the
160 traits include size and geometric features such as morphological complexity, as well as the
161 elongation and direction of an ellipse fitted to each fire patch. We considered only fire
162 patches ≥ 300 ha, because of the inaccurate morphologies of smaller patches (Nogueira et
163 al., 2017), and higher omission and commission errors for small fires in burned-area
164 products both globally (Padilla et al., 2015; Randerson et al., 2012; Roteta et al., 2019), and
165 in North America (Sparks et al., 2015).

166 *2.1.2. Reference data*

167 As reference data, we used fire patches from the Canadian National Fire Database (CNFD;
168 Canadian Forest Service, 2014) and the Wildland Fire Perimeters Database (WFPD; U.S.
169 Geological Survey, 2017) recorded during the 2005–2011 period coincident with the FRY
170 products. CNFD and WFPD provide homogeneous high spatial resolution daily fire-patch
171 data collected by different agencies from ground measurements, aerial products or high-
172 resolution satellite sensors. They have been used previously as reference data for validation
173 exercises based on their standard data assemblage protocol over North America (Chuvieco
174 et al., 2018). We checked both CNFD and WFPD fire patches to remove fire duplicates at
175 interstate borders or the border between the United States and Canada, and those recorded
176 by different agencies within the same country. Similarly, we also removed fire patches from
177 WFPD empirically drawn as circles around active fires identified by MODIS sensors. We also
178 grouped into a common patch some fires that had been split into spatially distinct patches in
179 these databases; this process makes them compatible with the way FRY treats patches. To
180 create the reference data, we rasterized CNFD and WFPD fire patches ≥ 300 ha to the
181 spatial resolutions of each FRY product (i.e., 300 m and 500 m), and derived their functional
182 traits following the same approach as in FRY (Laurent et al., 2018a).

183 *2.2. Functional diversity trait-based approach*

184 To assess the agreement between the FRY products and the reference data, we adopted
185 the functional diversity trait-based statistical framework proposed by Mouillot et al. (2013)
186 and Villéger et al. (2013, 2008). This approach was initially developed in functional ecology
187 to compare ecological communities (assemblages of individuals defined by their functional
188 traits and abundances) based on functional traits (i.e., characteristics of organisms related
189 by their functions, e.g., plant height for light interception; Garnier et al., 2016). We applied
190 this framework to compare fire-patch products by considering each fire-patch product as a
191 community and each fire patch as an individual defined by its morphological traits. This
192 approach complements the usual omission and commission errors performed for accuracy
193 assessment. Low commission and omission errors ensure most burned pixels are identified,
194 and in turn, that fire patched overlap between products. Comparing fire-patch morphology
195 reinforces this information by quantifying how the remaining small omission and commission
196 errors affect burned pixels at the fire-patch boundary and in turn modify fire shapes. The
197 approach includes four steps (Fig. 1).



198

199 **Fig. 1:** Theoretical functional diversity trait-based approach adapted from Moullot et al.
 200 (2013) and Villéger et al. (2013, 2008) to assess satellite-derived fire patches in four steps.
 201 Functional trait (F_{trait}) is a morphological feature of the fire patch. Functional diversity indices
 202 (FDIs) include functional fire-patch number (F_{fp}), functional richness (F_{ric}) and functional

203 dispersion (F_{dis}). Continental scale tile-to-tile Standardized Major Axis (SMA) regression of
204 FDIs, and tile-level functional beta diversity (F_{β}), functional turnover (F_{turn}) and functional
205 nestedness (F_{nest}) were used in the assessment. For a simple graphical display, the first step
206 shows tiles from only one product and the reference data. Similarly, the second, third and
207 fourth steps show a functional space. This space has only two functional traits in one tile; in
208 addition, the third step- F_{ric} and the fourth steps show convex hull volumes as a circle. A
209 Venn diagram illustrates these cases.

210 *2.2.1. First step: sample the fire-patch products*

211 To sample the fire-patch products by 2° tiles across the continent, we grouped the list of fire
212 patches belonging to a set of 10 products according to their central geographic coordinates
213 into $2^{\circ} \times 2^{\circ}$ spatial tiles (Fig. 1; First step). This tile resolution allows us to get tiles with more
214 than three fire patches in each product and optimizes computing time. This method has
215 previously been used for global analysis (Hantson et al., 2015; Laurent et al., 2019). We
216 assigned the geographic coordinates of each tile (bottom left corner) over the entire sample
217 area as the tile ID name. Similarly, we used the cut-off values from each FRY product and
218 the spatial resolution from each reference data set as the product ID name.

219 *2.2.2. Second step: build the functional space*

220 To build the functional space of the fire patches for each satellite-derived product and cut-off
221 value within each tile, we selected the functional traits of size, elongation, and direction, from
222 the FRY database as the three essential non-correlated fire spread traits, which are
223 independent of pixel resolution (Fig. 1; Second step). Before building the multidimensional
224 Euclidean space, we normalized the functional traits of size and elongation applying the
225 Box-Cox method using the 'boxcofit' R function from the 'geoR' R library (Ribeiro and
226 Diggle, 2016). For size, the function became the reciprocal square root transformation, and
227 for elongation, the function became the exponential transformation.

228 Likewise, functional traits were overall standardized to generate a trait distribution with a
229 mean that equalled 0 and a variance that equalled 1 using the ‘decostand’ R function from
230 the ‘vegan’ R library (Oksanen et al., 2016). Standardizing implies that all traits are
231 considered equally important for the analysis and makes functional spaces comparable
232 within and across products. The three continuous transformed and scaled functional traits
233 were suitable for building the functional space without using ordination methods to reduce or
234 synthesize axes, as is required when using more than three dimensions (Maire et al., 2015).
235 Then, we located each fire patch according to its functional trait values into the functional
236 space built on the three selected functional trait axes. The method then compares the FRY
237 products with the reference data based on the dissimilarities between their functional
238 volumes.

239 *2.2.3. Third step: assessment of the functional structure*

240 To assess the functional structure of the fire-patch products, defined as the distribution of
241 individual fires in the functional space built within each tile and for each product, we first
242 computed three functional diversity indices:

- 243 • Functional fire-patch index is the number of patches per tile (Fig. 1; Third step- F_{fp}).
244 Accurately conserving functional fire patches from satellite-derived products means
245 that the pixel aggregation method accurately represents the fractionation of total
246 burned area into patch number. It complements the fire size distribution index widely
247 used in global (e.g., Hantson et al., 2015; Laurent et al., 2018a) and regional studies
248 (e.g., Malamud et al., 1998; Moreno et al., 2011).
- 249 • The functional richness is the convex hull volume in the functional space driven by
250 the range of extreme values of patch traits in a product (Fig. 1; Third step- F_{ric}).
251 Differences in functional richness between the products correspond to differences in
252 the convex hull volume upon gathering all the fire patches belonging to the product.
253 Conserving functional richness from satellite-derived products means that convex

254 hull volumes driven by extreme values on three traits (size, elongation and direction)
255 are accurately represented — and independently of the patch morphological features
256 inside this convex hull volume.

257 • Functional dispersion is the mean distance of individual fire patches to the average
258 position of all the fire patches in the multidimensional functional space (Fig. 1; Third
259 step- F_{dis}). The differences in functional dispersion represent differences in the
260 deviation of fire-patch trait values from the centre of the functional space filled by the
261 product. Conserving functional dispersion from satellite-derived products means that
262 the distribution of individual fire-patch traits within the functional space is accurately
263 represented, so we can expect same fire-patch morphologies beside the extreme
264 values as tested with functional richness.

265 The values of functional richness range between 0 and 1 because it is the proportion of the
266 functional space filled by the fire patches present in a product compared to the functional
267 space filled by all the fire patches present in all the products to be evaluated. Similarly,
268 functional dispersion ranges between 0 and 1 because it is scaled by the maximum value
269 possible considering all the fire patches present in a product. We computed both indices
270 using the 'dbFD' R function from the 'FD' R library (Laliberté et al., 2015; Laliberte and
271 Legendre, 2010).

272 We then regressed across tiles the functional diversity indices computed from each FRY
273 product against the ones computed from the reference data using the standardized major
274 axis (SMA) method (Warton et al., 2006) to assess their spatial extent. The aim here is to
275 test whether the continental pattern of fire diversity within tiles is conserved across the
276 products; and thus if satellite-derived pyrodiversity indices are robust indicators of fire
277 regimes. SMA error is measured perpendicular to the SMA line — not along the y-axis as in
278 ordinary least squares regression. It is the appropriate method for summarising a bivariate

279 relationship between products, given uncertainties in both global products (Boschetti et al.,
280 2019; Padilla et al., 2014) and forest service perimeters (e.g., Short, 2015, 2014).

281 Bivariate SMA lines with a squared correlation coefficient (r^2) that were significant at the 95%
282 level were inferred, assuming x and y observations are independent. The inference
283 consisted of testing if the slope equals 1 and the intercept equals 0 at the 95% significance
284 level. SMA lines were estimated and inferred using the 'sma' R function from the 'smatr' R
285 library (Warton et al., 2012) for each functional diversity index, of which functional fire-patch
286 number and dispersion were log₁₀-transformed for an approximately normal distribution.
287 Two additional SMA lines were estimated and inferred in the boreal and temperate regions
288 defined in the Global Fire Emission Database (GFED; Giglio et al., 2013) across North
289 America to further assess the relationships by region with potentially contrasting results
290 because of different longitudes and fire types.

291 We finally qualified the SMA lines to find the line of best fit following a statistical criterion
292 proposed previously to assess simulations (Mesplé et al., 1996) with five possible outcomes,
293 ordered by increasing bias: an unbiased relationship (slope ≈ 1 , intercept ≈ 0) when two
294 products entirely agree (Fig. 1; Third step-a); a constantly biased relationship (slope ≈ 1 ,
295 intercept $\neq 0$) when one product is systematically overestimating or underestimating the
296 other (Fig. 1; Third step-b); a proportionally biased relationship (slope $\neq 1$, intercept ≈ 0)
297 when one product gives values that are higher or lower than those from the other by an
298 amount that is proportional to the value of the observations (Fig. 1; Third step-c); and an
299 additional outcome, the combination of both a constantly and proportionally biased
300 relationship (slope $\neq 1$, intercept $\neq 0$; Fig. 1; Third step-d). We graded the lines of best fit
301 according to r^2 when several lines fall into the same outcome (Fig. 1; Third step-e). Finally,
302 no significant relationship occurs when the correlation is not significant ($p > 0.05$).

303 *2.2.4. Fourth step: assessment of the functional dissimilarity*

304 As a final step, we assessed the functional dissimilarity between fire-patch products within
305 tiles to capture whether or not two convex hull volumes entirely overlap (best agreement with
306 similar trait value range). We estimated and decomposed the functional beta diversity into its
307 two components of turnover and nestedness (Villéger et al., 2013; Figure 1; Fourth step):

308 • Functional beta diversity is the dissimilarity in convex hull volumes in the fire-patch
309 functional space between two products. It is the sum of functional turnover and
310 functional nestedness. Functional beta diversity equals 0 for perfect overlap (Fig. 1;
311 Fourth step-a) and equals 1 for a total mismatch. Between these two extremes,
312 different values of functional beta diversity result from different values of functional
313 turnover and functional nestedness (Fig. 1; Fourth step-e and f).

314 • Functional turnover is the proportion of convex hull volumes in the functional space
315 not shared between two products, driven by differences in trait values. When
316 functional beta diversity equals 0, functional turnover also equals 0 because the two
317 volumes perfectly overlap. When functional beta diversity equals 1, functional
318 turnover also equals 1, if the two similar convex hull volumes are in total mismatch
319 (Fig. 1; Fourth step-b and c), or equals 0 if one volume is included inside the other
320 one.

321 • Functional nestedness is the proportion of convex hull volumes in the functional
322 space shared between two products, driven by differences in functional richness.
323 Functional nestedness is the difference between functional beta diversity and
324 functional turnover. When functional beta diversity equals 1, functional nestedness
325 also equals 1 if one volume fills only a small portion of the other (Fig. 1; Fourth step-
326 d).

327 We computed functional beta diversity and its two components using the `all.intersect` R
328 function from the 'rcdd' R library (Geyer et al., 2017). Differences in functional dissimilarities
329 across cut-off values and within cut-off values were estimated using ANOVA analysis and

330 means were compared using Fisher's least significant difference test, both of them at the
331 95% significance level — these are available using the 'aov' R function from 'stats' R library
332 (R Core Team, 2017) and the 'LSD.test' R function from 'agricolae' R library (De Mendiburu,
333 2014).

334 **3. Results**

335 We show below how indices of fire-patch morphological trait diversity are conserved
336 between the satellite-derived products and the reference data across 141 tiles in North
337 America (mainland United State and Canada), including 68 tiles (48%) in Boreal North
338 America (BONA) and 73 tiles (52%) in Temperate North America (TENA).

339 *3.1. Functional structure*

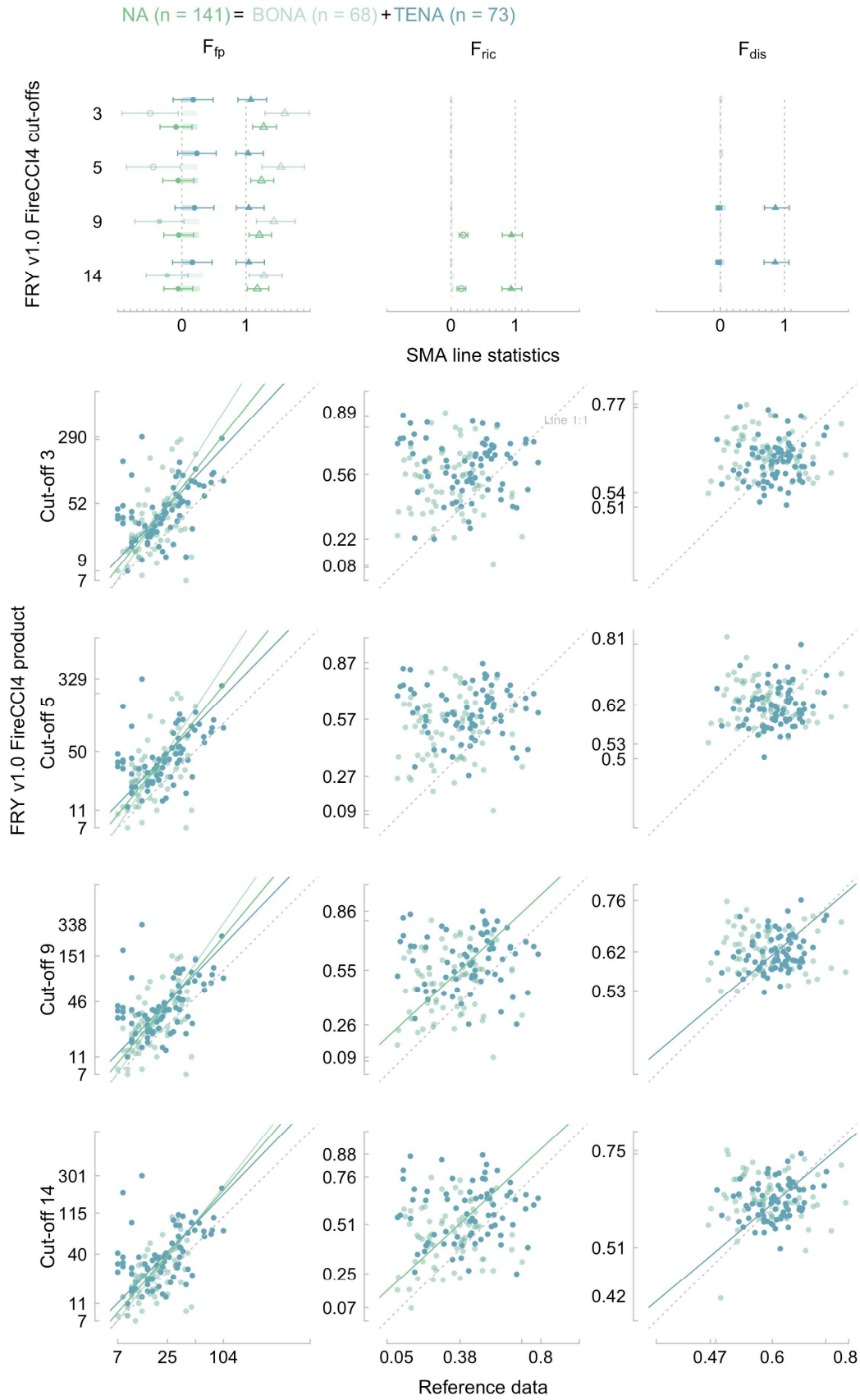
340 When we compared the functional diversity indices across tiles in North America between
341 the FRY products and the reference data, we found that the functional structure in the FRY-
342 MCD64A1 product was more correlated with the reference data and had smaller bias than
343 the FRY-FireCCI41 product (Figs. 2 and 3).

344 Functional fire-patch number relationships revealed significant correlations between the FRY
345 products and reference data across North America, BONA and TENA, with all the cut-off
346 values. Correlations with the reference data were stronger in the FRY-MCD64A1 product
347 than in the FRY-FireCCI41 product, particularly in BONA. In the FRY-MCD64A1 product r^2
348 varied from 0.21 to 0.45 ($p < 0.001$) whereas in the FRY-FireCCI41 product, r^2 varied from
349 0.20 to 0.33 ($p < 0.001$). Such relationships were all proportionally biased across North
350 America in both FRY products, but unbiased in both BONA and TENA in the FRY-MCD64A1
351 product, and unbiased only in TENA in the FRY-FireCCI41 product. In both FRY products,
352 correlations increased with increasing cut-off values across North America and BONA, but
353 decreased slightly with increasing cut-off values in TENA. Based on the higher r^2 ($p < 0.001$),
354 the line of best fit between both FRY products and the reference data was with a cut-off of
355 14 days across North America ($r^2 = 0.28$ and $r^2 = 0.31$ for the FRY-FireCCI41 and FRY-

356 MCD64A1 products respectively) and BONA ($r^2 = 0.33$ and $r^2 = 0.45$ for the FRY-FireCCI41
357 and FRY-MCD64A1 products respectively), whereas best fit was with a cut-off of 3 days in
358 TENA ($r^2 = 0.23$ and $r^2 = 0.29$ for the FRY-FireCCI41 and FRY-MCD64A1 products
359 respectively) as well as with cut-offs of 5 and 9 days in FRY-FireCCI41. In turn, fire-patch
360 number is well conserved in both FRY products with high cut-off values across North
361 America and BONA, yet small cut-off values in TENA. Overall, better performance was
362 found with the FRY-MCD64A1 product.

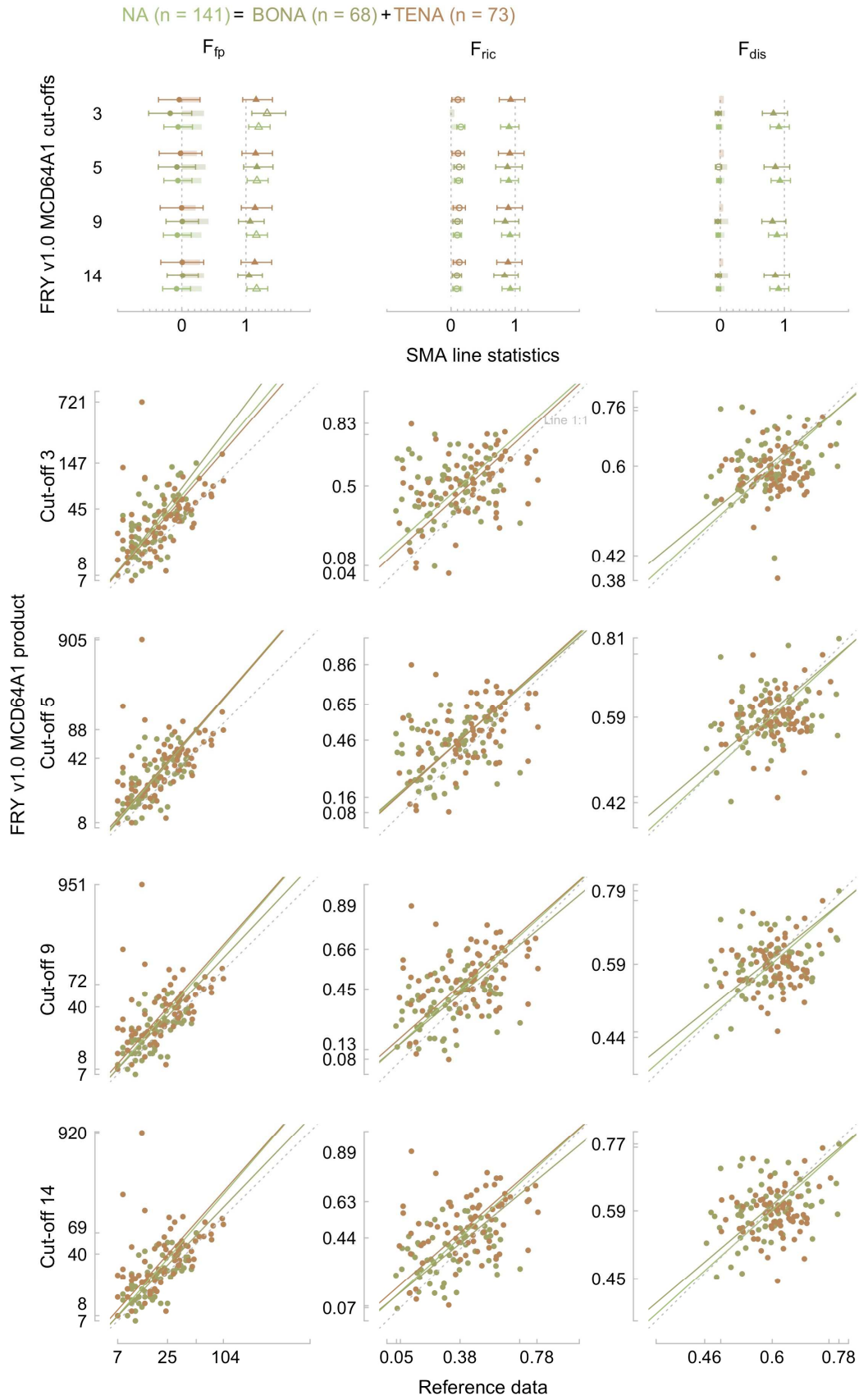
363 Continental functional richness relationships highlighted the differences between the FRY
364 products and reference data in the chosen 3D trait space. In the FRY-FireCCI41 product, r^2
365 varied from 0.04 to 0.03 ($p < 0.05$), and such weak relationships with the reference data
366 were significant only with cut-offs of 9 and 14 days across North America. In the FRY-
367 MCD64A1 product, r^2 varied from 0.08 to 0.19 ($p < 0.01$) and was significant with all cut-offs
368 across North America and TENA, and with cut-offs of above 5 days in BONA. In both FRY
369 products, all the relationships with the reference data were constantly biased, and the
370 correlations were stronger in the FRY-MCD64A1 product than in the FRY-FireCCI4 product.
371 Additionally, the correlations increased with increasing cut-off values across North America
372 and BONA but decreased slightly with increasing cut-off values in TENA. Based on the
373 higher r^2 ($p < 0.001$), the line of best fit between the FRY-MCD64A1 product and the
374 reference data was with a cut-off of 14 days across North America ($r^2 = 0.19$) and with cut-
375 offs of both 9 and 14 days in BONA ($r^2 = 0.15$), and with a cut-off of 3 days in TENA ($r^2 =$
376 0.15). Whereas the line of best fit between the FRY-FireCCI41 product and reference data
377 was with a cut-off of 14 days across North America ($r^2 = 0.04$). We conclude here that the 3D
378 volumes, driven by extreme values of fire size, elongation and direction, are less spatially
379 conserved than fire-patch number but still significant with better performances by the FRY-
380 MCD64A1 product with high cut-off values across North America and BONA as well as small
381 cut-off values in TENA.

382 Finally, functional dispersion relationships between the FRY products and the reference data
383 highlighted an additional better performance by the FRY-MCD64A1 product over FRY-
384 FireCCI41. In the FRY-FireCCI41 product, r^2 varied from 0.06 to 0.08 ($p < 0.05$), and such
385 relationships with the reference data were significantly correlated only with high cut-off
386 values in TENA. With the FRY-MCD64A1 product, values of r^2 were slightly higher, and
387 varied from 0.05 to 0.12 ($p < 0.05$). They were significant for all the cut-off values across
388 North America and BONA. In both FRY products, all the relationships with the reference
389 data were likewise unbiased. Furthermore, correlations increased with increasing cut-off
390 values across North America and BONA, but decreased slightly with increasing cut-off
391 values in TENA. Based on the higher r^2 ($p < 0.001$), the line of best fit between the FRY-
392 MCD64A1 product and the reference data was with a cut-off of 14 days across North
393 America ($r^2 = 0.07$), and with cut-offs of 9 and 14 days in BONA ($r^2 = 0.12$). However, the line
394 of best fit between the FRY-FireCCI41 product and reference data was with a cut-off of 9
395 days in TENA ($r^2 = 0.08$). We therefore conclude that the distribution of fire patches within
396 the 3D volumes conserves less information in the FRY products, but they are still significant
397 and the overall performance is better in the FRY-MCD64A1 product with high cut-off values.



398
 399 **Fig. 2.** Relationships of functional diversity indices between the FRY v1.0 FireCCI41 product
 400 and the reference data. Different colours identify data across tiles (n) in North America (NA),

401 Boreal North America (BONA) and Temperate North America (TENA). The left column refers
402 to the number of fire patches (F_{fp}), middle column to functional richness (F_{ric}) and the right
403 column to functional dispersion (F_{dis}). The upper panel shows the Standardized Major Axis
404 (SMA) line statistics. The squared correlation coefficient is represented by a rectangle and a
405 filled rectangle when it is significant ($p < 0.05$). In addition, for every significant squared
406 correlation coefficient, the SMA slope represented by a triangle and a filled triangle when it is
407 significant ($p > 0.05$), SMA intercept represented by a point and a filled point when it is
408 significant ($p > 0.05$), and confidence intervals at the 95% level are provided. The lower
409 panel shows the scatter plots with SMA lines for every significant squared correlation
410 coefficient ($p < 0.05$). The horizontal axis presents the functional diversity indices in the
411 reference data and the vertical axis in the FRY- FireCCI4 cut-off values. Both axes are in
412 log₁₀-scale for F_{fp} and F_{dis} . Each point is a 2° tile containing multiple patches.



413
 414 **Fig. 3.** Relationships of functional diversity indices between the FRY v1.0 MCD64A1 product
 415 and the reference data. Different colours identify data across tiles (n) in North America (NA),

416 Boreal North America (BONA) and Temperate North America (TENA). The left column refers
417 to the number of fire patches (F_{fp}), middle column to functional richness (F_{ric}) and the right
418 column to functional dispersion (F_{dis}). The upper panel shows the Standardized Major Axis
419 (SMA) line statistics. The squared correlation coefficient is represented by a rectangle and a
420 filled rectangle when it is significant ($p < 0.05$). In addition, for every significant squared
421 correlation coefficient, the SMA slope represented by a triangle and a filled triangle when it is
422 significant ($p > 0.05$), SMA intercept represented by a point and a filled point when it is
423 significant ($p > 0.05$), and confidence intervals at the 95% level are provided. The lower
424 panel shows the scatter plots with SMA lines for every significant squared correlation
425 coefficient ($p < 0.05$). The horizontal axis presents the functional diversity indices in the
426 reference data and the vertical axis in the FRY-MCD64A1 cut-off values. Both axes are in
427 log₁₀-scale for F_{fp} and F_{dis} . Each point is a 2° tile containing multiple patches.

428 *3.3. Functional dissimilarity*

429 We compared the overlap of functional spaces within tiles between FRY products and the
430 reference data, as a complementary indicator of functional similarities. We found that the
431 functional dissimilarities were lower between the FRY-MCD64A1 product and reference data
432 than between the FRY-FireCCI41 product and reference data (Figs. 4, 5, 6 and 7 and Table
433 S4). This result confirms the better performance of the FRY-MCD64A1 product in conserving
434 fire-patch morphology with more overlapping functional spaces.

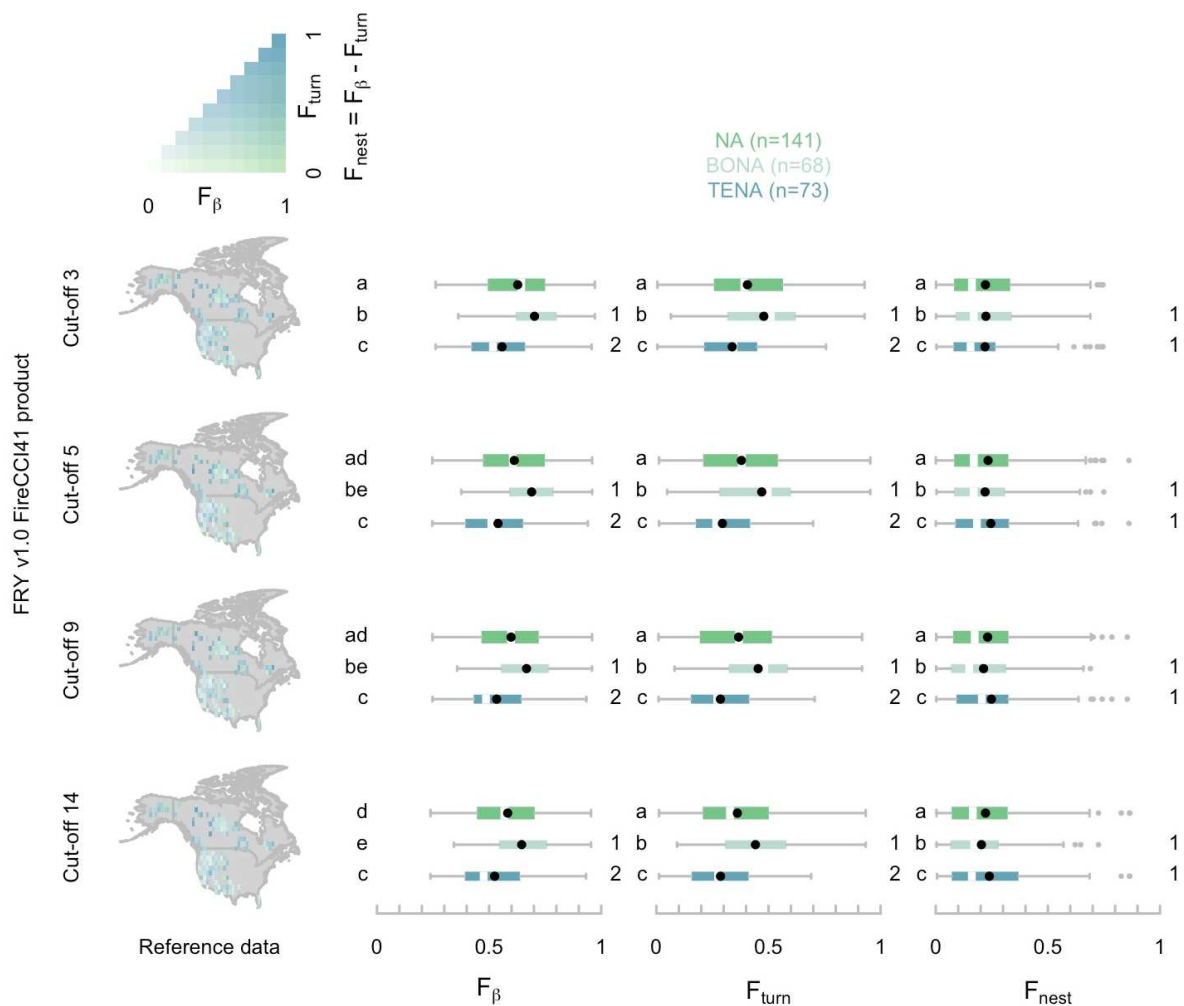
435 Functional beta diversity in the FRY-MCD64A1 product (beta diversity from 0.22 to 0.96)
436 was lower than in the FRY-FireCCI41 product (beta diversity from 0.24 to 0.97). That means
437 a higher overlap between functional spaces between the reference data and the FRY-
438 MCD64A1 product than between the reference data and the FRY-FireCCI41 product. In both
439 FRY products, the functional beta diversity was on average higher in BONA than in TENA
440 and significantly different ($p < 0.05$), indicating lower agreement with reference data in
441 BONA. For example, the overlap between functional spaces in California (Figs. 5 and 7 in

442 columns labelled California) on the 3 traits was higher than in Quebec (e.g., Figs. 5 and 7 in
443 columns labelled Quebec), particularly on the size axis when related to the fire-patch
444 elongation. We also found the functional beta diversity decreased with increasing cut-off
445 values in both FRY products across North America and BONA and TENA (Figs. 4 and 6).
446 That means an increase in the overlap between functional spaces. However, only in the
447 FRY-FireCCI41 product, was functional beta diversity derived from fire patches with a cut-off
448 of 3 days significantly lower ($p < 0.05$) than that with a cut-off of 14 days across North
449 America and in BONA.

450 In both FRY products, functional beta diversity was mostly driven by functional turnover,
451 indicating a low overlap of functional spaces between the FRY products and reference data;
452 this was due to a translation of functional spaces rather than the inclusion of a smaller one
453 into the other. We observed that functional turnover decreased with increasing cut-off
454 values, indicating higher overlap between functional spaces, and in turn, a better agreement
455 between functional spaces of fire patches generated with high cut-off values and functional
456 spaces generated with reference data. Furthermore, functional turnover was on average
457 also significantly ($p < 0.05$) higher in BONA than in TENA, thereby indicating lower
458 agreement with reference data in BONA. For example, on the size axis when related to the
459 elongation in Quebec (e.g., Figs. 5 and 7 in columns labelled Quebec) there is a tendency
460 for translation in functional spaces, especially in the FRY-FireCCI41 product. This tile in
461 Quebec in the FRY-MCD64A1 product is also a clear example of how functional
462 dissimilarities complement functional diversity indices. Here the two assemblages have
463 similar functional volumes and individual distribution in this volume but translated, thus
464 functional spaces do not overlap.

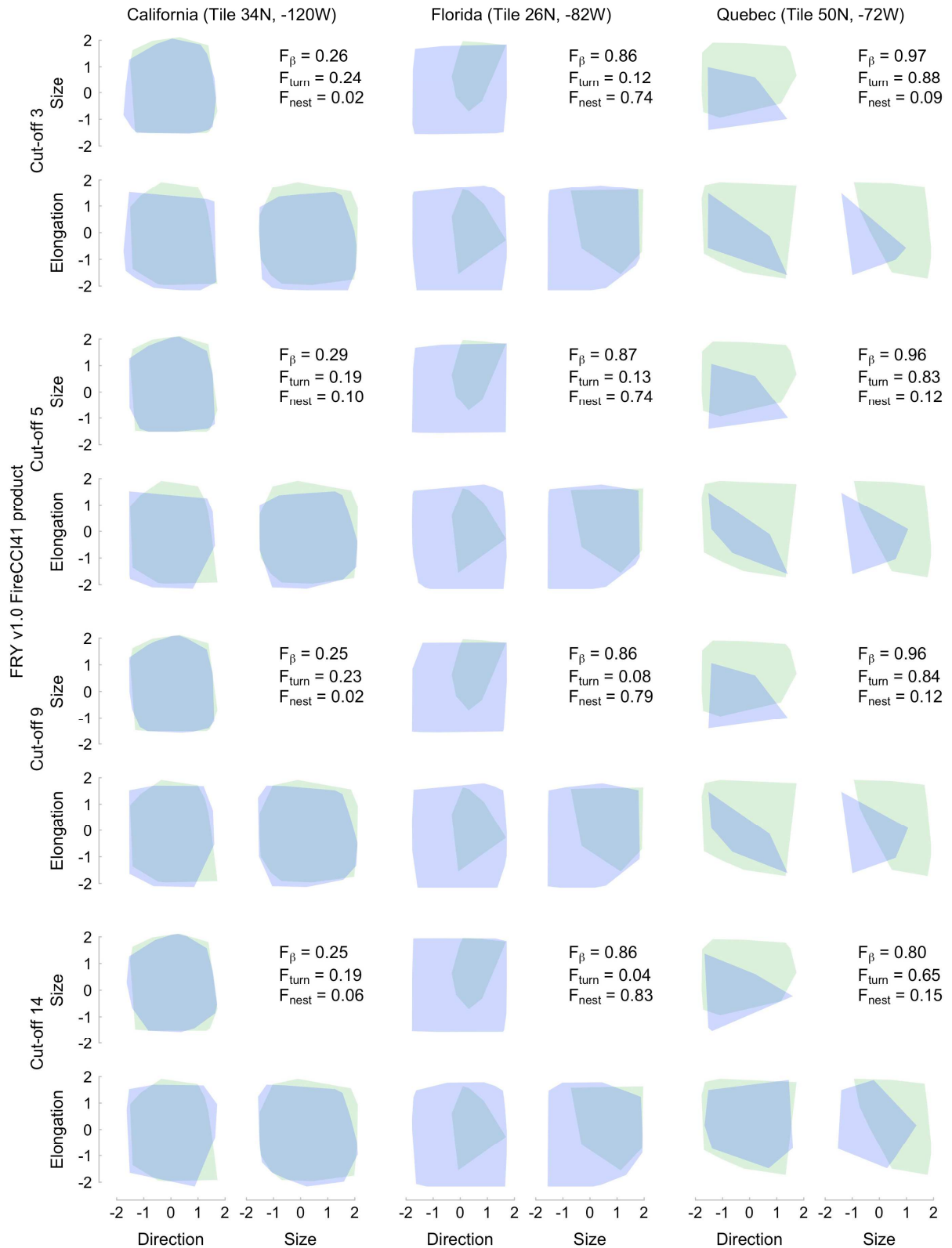
465 Functional nestedness varied slightly with cut-off values across North America but
466 decreased with increasing cut-off values in BONA and increased with increasing cut-off
467 values in TENA. This occurred in both FRY products, indicating the inclusion of one
468 functional space into the other and in agreement with decreasing turnover. While in the FRY-

469 FireCCI41 product functional nestedness on average was higher in TENA because of
 470 differences in functional richness between the product and reference data; in the FRY-
 471 MCD64A1 product, it varied slightly between regions. However, none of those differences
 472 were significant. For example, in Florida (e.g., Figs. 5 and 7 in columns labelled Florida),
 473 there are considerable differences in functional spaces due to their different volumes leading
 474 to the inclusion of the smaller volume of the reference data and thus a high nestedness.



475 **Fig. 4.** Functional dissimilarities within tiles between the FRY v1.0 FireCCI41 product and
 476 the reference data in North America (NA), Boreal North America (BONA) and Temperate
 477 North America (TENA). Functional beta diversity (F_β) is the sum of functional turnover (F_{turn})
 478 and functional nestedness (F_{nest}) as explained in the text. Means across cut-off values with
 479

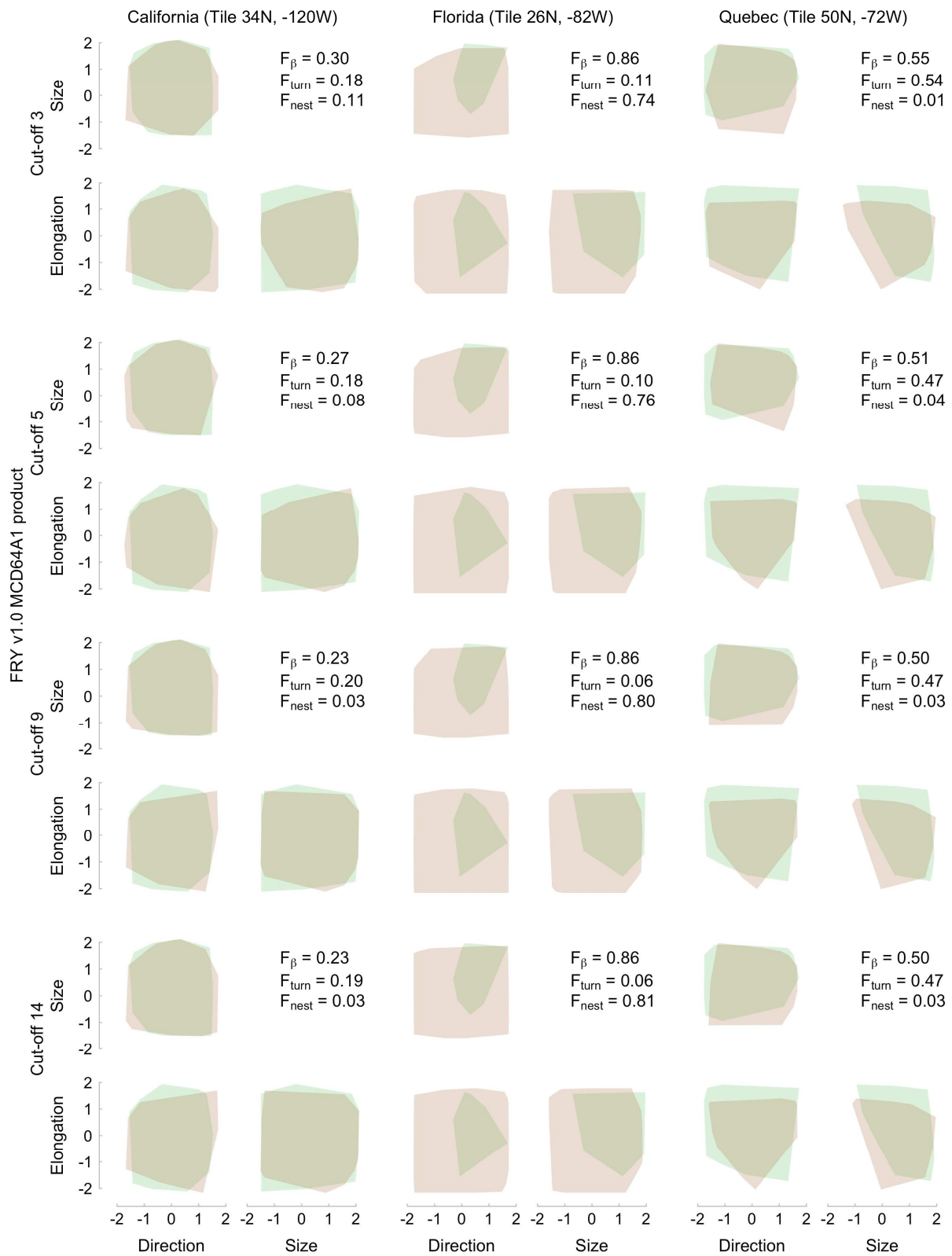
480 the same letter and means within cut-off values with the same number are not significantly
481 different ($p < 0.05$).



482
483

Fig. 5. Examples of functional dissimilarities within tiles between FRY v1.0 FireCCI41 (blue volume) and the reference data (green volume) in California (Tile 34N, -120W), Florida (Tile 26N, -82W) and Quebec (Tile 50N, -72W) for specific traits considered: size, direction,

484
485



496

497 **Fig. 7.** Examples of functional dissimilarities within tiles between FRY v1.0 MCD64A1 (red
 498 volume) and the reference data (green volume) in California (Tile 34N, -120W), Florida (Tile
 499 26N, -82W) and Quebec (Tile 50N, -72W) for specific traits considered: size, direction,

500 elongation of patches. Functional beta diversity (F_{β}) is the sum of functional turnover (F_{turn})
501 and functional nestedness (F_{nest}) as explained in the text.

502 **4. Discussion**

503 *4.1 A new statistical framework*

504 We evaluated the conservation of fire-patch morphology delivered in the satellite-derived
505 FRY database against reference data using a new functional trait-based approach. The
506 approach is a generic and synthetic surrogate to patch-patch regressions on morphological
507 traits (Andela et al., 2019; Chuvieco et al., 2018, 2016; Nogueira et al., 2017), and goes
508 beyond classical omission and commission errors (Fusco et al., 2019) used previously in
509 comparative pyrogeography.

510 Our approach has the advantage of assessing fire-patch accuracy using a synthetic view of
511 traits. Although here we built a functional space from three traits, more traits could be
512 included using ordination methods to reduce the data (Maire et al., 2015). However,
513 because the approach is sensitive to the addition of traits as well as to their correlations (Zhu
514 et al., 2017), it is, critical to make conscious decisions when selecting the traits (Gitay and
515 Noble, 1997). Here we selected three non-correlated essential traits related to fire spread.
516 We did not select functional traits of morphological complexity (e.g., perimeter/area ratio,
517 fractal dimension) as they are highly dependent on resolution.

518 The functional trait-based approach enables an assessment of satellite-derived fire patches
519 both across and within tiles, complementing each other. Across 2° tiles, it allows the
520 assessment of the spatial conservation of functional fire-patch diversity measured by
521 indices, such as functional fire patches, richness and dispersion between the two different
522 global satellite sensor products and the reference data. Within tiles, it allows the assessment
523 of the dissimilarities of functional diversity of fire-patch assemblages and detect where
524 mismatching occurs. Within tiles, we could also detect whether beta diversity was driven by

525 functional trait value differences or by richness differences. Although it is not a direct
526 outcome, it also allows us to explore which functional traits drive dissimilarities within tiles by
527 visual checking (e.g., Figs. 5 and 7).

528 In addition to fire patches, the approach proposed can be applied to assess emerging
529 satellite-derived trait products such as Essential Biodiversity Variables (EBVs; Kissling et al.,
530 2018; Pereira et al., 2013). The approach is also suitable for large- and small-scale
531 (Carmona et al., 2016) pyrogeography studies such as the recent study of Africa by
532 Hempson et al. (2018). The availability of fire-patch traits (Laurent et al., 2018a), is opening
533 up a new field of research on functional pyrogeography, by linking biogeography and
534 landscape ecology indices within a functional ecology statistical framework.

535 *4.2 Optimal cut-off values for fire-patch morphology*

536 The primary outcome of our analysis is that satellite-derived fire-patch morphology
537 conservation varied with the cut-off value. Out of the four cut-off values assessed, high cut-
538 off values generated fire patches with morphologies closest to the reference data in North
539 America and particularly in BONA (Figs. 2, 3, 4 and 6, and Table S4). However, in TENA,
540 the correlations slightly decreased with increasing cut-off values, but differences were not
541 significant. Still, the unexpected decrease of correlation with increasing cut-off values in
542 TENA in the FRY products may be because small fires, such as sugarcane fires in Florida
543 (McCarty et al., 2009) mistakenly reached the threshold of 300 ha with increasing cut-off
544 values (Figs. S1, S3, S5, and S7, and Tables S1 and S2), but were unreported in the
545 reference data (Figs. S9, S11, S13 and S14, and Table S3). Additionally, the omission and
546 commission errors of satellite-derived burned-area products (Boschetti et al., 2019; Padilla
547 et al., 2014; Randerson et al., 2012; Roteta et al., 2019), together with the uncertainties in
548 the date-of-burning, can cause fragmentation of large fires leading to more fire patches
549 (Figs. S13, S14, S15 and S16), and thus weak structural relationships between the FRY
550 products and reference data. Furthermore, the functional dissimilarities were lower on

551 average with a cut-off of 14 days across North America and in BONA and TENA (Figs. 4 and
552 6, and Table S4). Previous observations led to an estimated cut-off of 10 days in the same
553 regions, which was the highest of the assessed values (4, 6, 8, and 10 days; Andela et al.,
554 2019), and is in agreement with our results.

555 Fire-patch conservation also varied with region. For a given cut-off value, functional
556 dissimilarities of FRY products with reference data were higher in BONA than TENA.
557 Interestingly, the spatial relationships on functional structure (Figs. 2 and 3) were stronger in
558 BONA than in TENA. That means that despite presenting a similar regional pattern of
559 functional fire-patch diversity values between the FRY products and the reference data,
560 functional fire-patch traits were regionally dissimilar.

561 For example, in the FRY-MCD64A1 product, functional richness was constantly biased
562 across North America and in BONA and TENA (Fig. 3), and functional dissimilarities were
563 higher because of trait value differences (Fig. 6 and Table S4). Those trait value differences,
564 particularity for extremes, were more notable in BONA (e.g., Figs. 5 and 7 in Quebec and
565 Figs. S13 and S14). In contrast, functional dissimilarities driven by functional richness
566 differences and thus convex hull volume differences were more notable in TENA (e.g., Figs.
567 5 and 7 in columns labelled Florida and Figs. S13 and S14), showing contrasting
568 performances on fire-patch morphology conservation between BONA and TENA. The fact
569 that the functional turnover contributed more on average than functional nestedness also
570 supports that result (e.g., Figs. 5 and 7 in columns labelled Quebec). This result based on
571 our new statistical framework agrees well with previous studies using products of burned
572 area (e.g., Andela et al., 2019; Hantson et al., 2015) and active fire (Oom et al., 2016) for
573 fire-patch identification, arguing that the suitability of cut-off values can change regionally.

574 *4.3 High temporal resolution for fire-patch morphology*

575 We found that the MODIS sensors with the highest temporal resolution better capture fire-
576 patch morphology than the MERIS sensor that has a higher spatial resolution. Fire patches

577 in the FRY-MCD64A1 product based on MODIS sensors with a temporal resolution of 1 day
578 were closer to the reference data than in the FRY-FireCCI41 product (Figs. 4 and 5, and
579 Table S4) based on the MERIS sensor that had a temporal resolution of 3 days.
580 Furthermore, the FRY-MCD64A1 product showed a stronger spatial correlation of the
581 functional structure (Fig. 3) and lower functional dissimilarities (Fig. 6, and Table S4) with the
582 reference data than the FRY-FireCCI41 product (Figs. 4 and 5, and Table S4). For example,
583 in BONA, where fires tend to be extensive and spread for weeks and even months (Wang et
584 al., 2014), fire-patch morphology was better conserved in the FRY-MCD64A1 product than
585 in the FRY-FireCCI41 product (Figs. 2 and 3, and Figs. 5 and 7 in columns labelled
586 Quebec), in which uncertainties in the date-of-burning at the pixel-level in the raw data can
587 make large fires appear fragmented (Figs. S13 and S14).

588 Our results suggest that high temporal resolution reduces uncertainties in the date-of-
589 burning in fast-spreading fires (e.g., grassland fires) or short duration fires (e.g., cropland
590 fires or fires near human settlements where firefighters react quickly). For example, fire
591 patch number in the FRY-FireCCI41 product related to cropland fires in Idaho and, in
592 particular, sugarcane fires in Florida (McCarty et al., 2009) (Figs. S1, S3, and S13 and Table
593 S1) were approximately one-third of those in the FRY-MCD64A1 product (Figs. S5, S7 and
594 S14, and Table S2). These results suggest that the number of burned pixels in these
595 cropland systems are higher in FRY-FireCCI41 and affects patch assemblage.

596 No other studies have assessed the fire patches derived from the same two burned-area
597 products used here. However, they have been assessed for the MCD64A1 product alone
598 (Andela et al., 2019; Fusco et al., 2019) and for previous versions of both products
599 (Nogueira et al., 2017) in which the results from the two satellite sensors depended on traits.
600 Our assessment agrees well with the results of the validation of those burned-area products
601 (Padilla et al., 2014). Thus, satellite sensors with high temporal resolutions are more likely to
602 characterize fire patches accurately and thus would be a more cost-effective observation
603 system to consider in future ECV requirement updates (Mouillot et al., 2014; WMO, 2016).

604 This result implies that the low temporal resolution MERIS sensor should be abandoned in
605 the newly delivered FireCCI51 burned-area product. A merger of the high temporal
606 resolution data from the MODIS sensors at its highest spatial resolution of 250 m should
607 now act as the reference ESA Fire CCI product (Chuvieco et al., 2018).

608 4.4. Uncertainties and the way forward

609 We obtained low correlations between the functional diversity indices derived from the
610 satellite-derived FRY products and reference data. This result causes us to question both
611 the quality of the burned-area products at the pixel-level and the fire patches that resulted
612 from the pixel aggregation flood-fill algorithm. Despite being widely used as the only
613 homogeneous source of global information on burned area, spatial intercomparisons of
614 satellite-derived burned-area products (Humber et al., 2018) with satellite-derived reference
615 data based on fine-scale (Boschetti et al., 2019, 2016; Rodrigues et al., 2019; Sparks et al.,
616 2015) or local inventories (Fusco et al., 2019; Turco et al., 2019), remain spatially poorly
617 correlated regarding burned area only, with intrinsic theoretical uncertainty varying between
618 12.78% and 13.90% in TENA and between 53.53% and 65.87% in BONA (Brennan et al.,
619 2019). Thus, we expected a low correlation between observations and fire-patch
620 morphology; this expectation was based on the already low spatial correlation between the
621 data and the burned-area products, and significant commission and omission errors in both
622 the MCD64A1 (Boschetti et al., 2019) and FireCCI41 (Padilla et al., 2015) burned-area
623 products. Yet we still find that our correlation coefficients capture a realistic estimation of the
624 agreement on fire-patch morphologies. Fire-patch morphologies are more sensitive to
625 omission and commission errors at the pixel level, but produce different fire shapes as a
626 consequence of boundary misrepresentation (Humber et al., 2019). Thus, we suggest that,
627 besides increasing the effort in detecting small missing fires (e.g., Roteta et al., 2019), more
628 effort should be devoted to better boundary delimitation.

629 We attribute this low agreement to remaining uncertainties on the date-of-burning and fire
630 location at the pixel-level in the raw satellite data, but we also acknowledge issues in the
631 reference data (e.g., Short, 2015, 2014) and discrepancies in pixel-aggregation methods
632 (Andela et al., 2019; Artés et al., 2019; Campagnolo et al., 2019; Oom et al., 2016). The
633 flood-fill algorithm used in FRY (Laurent et al., 2018a) can over-aggregate pixels, and fail to
634 split concomitant fire-starts merging into one final single fire patch. This phenomenon is
635 most likely to occur in a savanna ecosystem, so we would expect it to occur less frequently
636 in North America (Oom et al., 2016). However, we anticipate improvements in fire patch
637 delineation to result from a more efficient method of pixel aggregation — new satellite-
638 derived fire patches are still emerging.

639 The trait-based approach used here has been widely used in community ecology over the
640 past few decades (Chao et al., 2019). Gitay and Noble (1997) have discussed the critical
641 issues regarding the choice of traits to consider and how to seek them; Maire et al. (2015)
642 the sensitivity of indices to the selection and reduction of traits; and Zhu et al. (2017) heir
643 correlations. We acknowledge that combining the assessments of the functional structures
644 and dissimilarities is crucial because fire-patch assemblages can lead to similar functional
645 diversity indices (Chao et al., 2019). Furthermore, by using complementary indices as we
646 did, it is possible to efficiently differentiate assembly processes (Münkemüller et al., 2012).

647 For future trait-based assessments, we suggest both the spatial location and date-of-burning
648 of fire patches should be considered as essential fire regime traits. Although we omitted the
649 spatial location of the fire patches from our analysis, that was because we expected low
650 commission and omission errors at the boundaries of fire patches, i.e., we assumed that
651 most overlapping patches would be captured, an assumption based on the work of Nogueira
652 et al. (2017), who found more than 70% of fire patches to be ≥ 300 ha identified. For
653 example, Hempson et al. (2018) considered the fire return interval as a trait to examine the
654 spatial and temporal overlap between patches and Wiegand et al. (2017) implemented the

655 spatial location of individuals in plant diversity. Fire return interval can thus be used for more
656 comprehensive regional pyrodiversity analysis.

657 Although our approach benefits from its versatility across scales (Carmona et al., 2016), the
658 sensitivity analysis of tile size by biome remains for future studies. For example, Matthews et
659 al. (2019) explored the species-area relationships to determine the spatial resolution
660 capturing all species types. Similarly, Turco et al. (2019) observed that increasing tile
661 resolution improved correlations between satellite-derived burned area and reference data in
662 Europe.

663 Despite those limitations, the functional trait-based approach proposed here presents a
664 significant advance in fire patch trait assessment — it allows a comprehensive assessment
665 of fire spread diversity to be derived from the FRY products across North America.

666 **5. Conclusions**

667 We implemented and tested the efficiency of a functional trait-based approach for the new
668 topic of satellite-derived fire-patch morphology assessment. We showed that this method
669 can be used for assessing satellite-derived fire patches beyond assessments based on
670 commission and omission errors in satellite-derived burned-area products. The approach
671 relies on fire-patch traits and with just a few indices can synthesize an intercomparison of
672 burned-area products or pyroregions. The approach opens up a new and promising field of
673 research.

674 These results demonstrate that the more reliable fire-patch maps can be created by using a
675 fixed cut-off value — in North America that cut-off value is 14 days. Furthermore, satellite
676 sensor monitoring at a higher temporal resolution will lead to improvements in burned-area
677 mapping and the identification of fire patches; thus, high frequency monitoring from satellites
678 is the most cost-effective climate observation system.

679 Using this trait-based approach, we can assess burned-area products at the pixel level —
680 assessments that will underpin pyrogeographical analysis and model benchmarking through
681 the emerging topic of fire-patch identification and the related fire-patch properties such as
682 fire size and fire spreading.

683 **Acknowledgements**

684 The ESA Fire_cci project [Contract N° 4000115006/15/I-NB] supported this research and P.
685 Laurent's work. M.V. Moreno's work was supported by UM Post-Doc programme co-
686 financed by the ESA Fire_cci project, and an IRD post-doctoral fellowship. We thank D.
687 Mouillot for his feedback on the methodology and results. We also thank the forest services
688 for providing information about the fire perimeters used in this study.

689 **References**

- 690 Andela, N., Morton, D.C., Giglio, L., Paugam, R., Chen, Y., Hantson, S., van der Werf, G.R.,
691 Randerson, J.T., 2019. The Global Fire Atlas of individual fire size, duration, speed and
692 direction. *Earth Syst. Sci. Data* 11, 529–552. <https://doi.org/10.5194/essd-11-529-2019>
- 693 Andreae, M.O., 2019. Emission of trace gases and aerosols from biomass burning – an
694 updated assessment. *Atmos. Chem. Phys.* 19, 8523–8546. [https://doi.org/10.5194/acp-](https://doi.org/10.5194/acp-19-8523-2019)
695 [19-8523-2019](https://doi.org/10.5194/acp-19-8523-2019)
- 696 Andreae, M.O., Merlet, P., 2001. Emission of trace gases and aerosols from biomass
697 burning. *Global Biogeochem. Cycles* 15, 955–966.
698 <https://doi.org/10.1029/2000GB001382>
- 699 Archibald, S., Roy, D.P., 2009. Identifying individual fires from satellite-derived burned area
700 data, in: *International Geoscience and Remote Sensing Symposium (IGARSS)*. pp. III-
701 160-III–163. <https://doi.org/10.1109/IGARSS.2009.5417974>
- 702 Artés, T., Oom, D., de Rigo, D., Durrant, T.H., Maianti, P., Libertà, G., San-Miguel-Ayanz, J.,
703 2019. A global wildfire dataset for the analysis of fire regimes and fire behaviour. *Sci.*

704 Data 6, 296. <https://doi.org/10.1038/s41597-019-0312-2>

705 Bistinas, I., Harrison, S.P., Prentice, I.C., Pereira, J.M.C., 2014. Causal relationships versus
706 emergent patterns in the global controls of fire frequency. *Biogeosciences* 11, 5087–
707 5101. <https://doi.org/10.5194/bg-11-5087-2014>

708 Boschetti, L., Brivio, P.A., Eva, H.D., Gallego, J., Baraldi, A., Gregoire, J., 2006. A sampling
709 method for the retrospective validation of global burned area products. *IEEE Trans.*
710 *Geosci. Remote Sens.* 44, 1765–1773. <https://doi.org/10.1109/TGRS.2006.874039>

711 Boschetti, L., Roy, D.P., Giglio, L., Huang, H., Zubkova, M., Humber, M.L., 2019. Global
712 validation of the collection 6 MODIS burned area product. *Remote Sens. Environ.* 235,
713 111490. <https://doi.org/10.1016/j.rse.2019.111490>

714 Boschetti, L., Stehman, S. V., Roy, D.P., 2016. A stratified random sampling design in space
715 and time for regional to global scale burned area product validation. *Remote Sens.*
716 *Environ.* <https://doi.org/10.1016/j.rse.2016.09.016>

717 Boschetti, L.R.D., Justice, C., 2009. International Global Burned Area Satellite Product
718 Validation Protocol. Part I - Production and standardization of validation reference data,
719 In CEOS-Ca. ed. USA: Committee on Earth Observation Satellites.

720 Bowman, D.M.J.S., Balch, J.K., Artaxo, P., Bond, W.J., Carlson, J.M., Cochrane, M.A.,
721 D\textquoterightAntonio, C.M., DeFries, R.S., Doyle, J.C., Harrison, S.P., Johnston,
722 F.H., Keeley, J.E., Krawchuk, M.A., Kull, C.A., Marston, J.B., Moritz, M.A., Prentice,
723 I.C., Roos, C.I., Scott, A.C., Swetnam, T.W., van der Werf, G.R., Pyne, S.J., 2009. Fire
724 in the Earth System. *Science*. 324, 481–484. <https://doi.org/10.1126/science.1163886>

725 Brennan, J., Gómez-Dans, J.L., Disney, M., Lewis, P., 2019. Theoretical uncertainties for
726 global satellite-derived burned area estimates. *Biogeosciences* 16, 3147–3164.
727 <https://doi.org/10.5194/bg-16-3147-2019>

728 Campagnolo, M.L., Oom, D., Padilla, M., Pereira, J.M.C., 2019. A patch-based algorithm for
729 global and daily burned area mapping. *Remote Sens. Environ.* 232, 111288.

730 <https://doi.org/10.1016/j.rse.2019.111288>

731 Canadian Forest Service, 2014. Canadian National Fire Database – Agency Fire Data.
732 Natural Resources Canada, Northern Forestry Centre, Edmonton, Alberta. Canada.
733 <http://cwfis.cfs.nrcan.gc.ca/ha/nfdb>.

734 Carmona, C.P., de Bello, F., Mason, N.W.H., Lepš, J., 2016. Traits Without Borders:
735 Integrating Functional Diversity Across Scales. *Trends Ecol. Evol.* 31, 382–394.
736 <https://doi.org/10.1016/j.tree.2016.02.003>

737 Chao, A., Chiu, C.-H., Villéger, S., Sun, I.-F., Thorn, S., Lin, Y.-C., Chiang, J.-M., Sherwin,
738 W.B., 2019. An attribute-diversity approach to functional diversity, functional beta
739 diversity, and related (dis)similarity measures. *Ecol. Monogr.* 89, e01343.
740 <https://doi.org/10.1002/ecm.1343>

741 Chuvieco, E., Lizundia-Loiola, J., Lucrecia Pettinari, M., Ramo, R., Padilla, M., Tansey, K.,
742 Mouillot, F., Laurent, P., Storm, T., Heil, A., Plummer, S., 2018. Generation and
743 analysis of a new global burned area product based on MODIS 250 m reflectance
744 bands and thermal anomalies. *Earth Syst. Sci. Data* 10, 2015–2031.
745 <https://doi.org/10.5194/essd-10-2015-2018>

746 Chuvieco, E., Yue, C., Heil, A., Mouillot, F., Alonso-Canas, I., Padilla, M., Pereira, J.M.,
747 Oom, D., Tansey, K., 2016. A new global burned area product for climate assessment
748 of fire impacts. *Glob. Ecol. Biogeogr.* 25, 619–629. <https://doi.org/10.1111/geb.12440>

749 De Mendiburu, F., 2014. *Agricolae: Statistical procedures for agricultural research*. R
750 package version 1.2-0. <http://CRAN.R-project.org/package=agricolae>.

751 Fusco, E.J., Finn, J.T., Abatzoglou, J.T., Balch, J.K., Dadashi, S., Bradley, B.A., 2019.
752 Detection rates and biases of fire observations from MODIS and agency reports in the
753 conterminous United States. *Remote Sens. Environ.* 220, 30–40.
754 <https://doi.org/10.1016/j.rse.2018.10.028>

755 Garnier, E., Navas, M.-L., Grigulis, K., 2016. Plant Functional Diversity, Plant Functional

756 Diversity. Oxford University Press.
757 <https://doi.org/10.1093/acprof:oso/9780198757368.001.0001>

758 Geyer, C.J., Meeden, G.D., Fukuda, K., 2017. rccd: Computational Geometry. R package
759 version 1.2.

760 Giglio, L., Boschetti, L., Roy, D.P., Humber, M.L., Justice, C.O., 2018. The Collection 6
761 MODIS burned area mapping algorithm and product. *Remote Sens. Environ.* 217, 72–
762 85. <https://doi.org/10.1016/j.rse.2018.08.005>

763 Giglio, L., Randerson, J.T., van der Werf, G.R., 2013. Analysis of daily, monthly, and annual
764 burned area using the fourth-generation global fire emissions database (GFED4). *J.*
765 *Geophys. Res. Biogeosciences* 118, 317–328. <https://doi.org/10.1002/jgrg.20042>

766 Giglio, L., Schroeder, W., Justice, C.O., 2016. The collection 6 MODIS active fire detection
767 algorithm and fire products. *Remote Sens. Environ.* 178, 31–41.
768 <https://doi.org/10.1016/j.rse.2016.02.054>

769 Gitay, H., Noble, I., 1997. What are functional types and how should we seek them?, in:
770 Smith TM, Shugart HH, W.F. (Ed.), *Plant Functional Types: Their Relevance to*
771 *Ecosystem Properties and Global Change*. Cambridge University Press, Cambridge,
772 pp. 3–19.

773 Hantson, S., Arneth, A., Harrison, S.P., Kelley, D.I., Colin Prentice, I., Rabin, S.S., Archibald,
774 S., Mouillot, F., Arnold, S.R., Artaxo, P., Bachelet, D., Ciais, P., Forrest, M.,
775 Friedlingstein, P., Hickler, T., Kaplan, J.O., Kloster, S., Knorr, W., Lasslop, G., Li, F.,
776 Mangeon, S., Melton, J.R., Meyn, A., Sitch, S., Spessa, A., van der Werf, G.R.,
777 Voulgarakis, A., Yue, C., 2016. The status and challenge of global fire modelling.
778 *Biogeosciences* 13, 3359–3375. <https://doi.org/10.5194/bg-13-3359-2016>

779 Hantson, S., Pueyo, S., Chuvieco, E., 2015. Global fire size distribution is driven by human
780 impact and climate. *Glob. Ecol. Biogeogr.* 24, 77–86. <https://doi.org/10.1111/geb.12246>

781 Hempson, G.P., Parr, C.L., Archibald, S., Anderson, T.M., Mustaphi, C.J.C., Dobson, A.P.,

782 Donaldson, J.E., Morrison, T.A., Probert, J., Beale, C.M., 2018. Continent-level drivers
783 of African pyrodiversity. *Ecography*. 41, 889–899. <https://doi.org/10.1111/ecog.03109>

784 Humber, M.L., Boschetti, L., Giglio, L., 2019. Assessing the Shape Accuracy of Coarse
785 Resolution Burned Area Identifications. *IEEE Trans. Geosci. Remote Sens.* 1–11.
786 <https://doi.org/10.1109/TGRS.2019.2943901>

787 Humber, M.L., Boschetti, L., Giglio, L., Justice, C.O., 2018. Spatial and temporal
788 intercomparison of four global burned area products. *Int. J. Digit. Earth*.
789 <https://doi.org/10.1080/17538947.2018.1433727>

790 Kissling, W.D., Walls, R., Bowser, A., Jones, M.O., Kattge, J., Agosti, D., Amengual, J.,
791 Basset, A., van Bodegom, P.M., Cornelissen, J.H.C., Denny, E.G., Deudero, S., Egloff,
792 W., Elmendorf, S.C., Alonso García, E., Jones, K.D., Jones, O.R., Lavorel, S., Lear, D.,
793 Navarro, L.M., Pawar, S., Pirzl, R., Rüger, N., Sal, S., Salguero-Gómez, R., Schigel, D.,
794 Schulz, K.-S., Skidmore, A., Guralnick, R.P., 2018. Towards global data products of
795 Essential Biodiversity Variables on species traits. *Nat. Ecol. Evol.* 2, 1531–1540.
796 <https://doi.org/10.1038/s41559-018-0667-3>

797 Laliberte, E., Legendre, P., 2010. A distance-based framework for measuring functional
798 diversity from multiple traits. *Ecology* 91, 299–305. <https://doi.org/10.1890/08-2244.1>

799 Laliberté, E., Legendre, P., Shipley, B., 2015. FD: measuring functional diversity from
800 multiple traits, and other tools for functional ecology. *R Packag.* Version 1.0-12.

801 Laurent, P., Mouillot, F., Moreno, M. V, Yue, C., Ciais, P., 2019. Varying relationships
802 between fire radiative power and fire size at a global scale. *Biogeosciences* 16, 275–
803 288. <https://doi.org/10.5194/bg-16-275-2019>

804 Laurent, P., Mouillot, F., Yue, C., Ciais, P., Moreno, M.V., Nogueira, J.M.P., 2018a. FRY, a
805 global database of fire patch functional traits derived from space-borne burned area
806 products. *Sci. Data* 5, 180132. <https://doi.org/10.1038/sdata.2018.132>

807 Laurent, P., Mouillot, F., Yue, C., Ciais, P., Moreno, M.V., Nogueira, J.M.P., 2018b. FRY: a

808 global database of fire patch functional traits. <https://doi.org/10.15148/0e999ffc-e220->
809 [41ac-ac85-76e92ecd0320](https://doi.org/10.15148/0e999ffc-e220-41ac-ac85-76e92ecd0320)

810 Maire, E., Grenouillet, G., Brosse, S., Villéger, S., 2015. How many dimensions are needed
811 to accurately assess functional diversity? A pragmatic approach for assessing the
812 quality of functional spaces. *Glob. Ecol. Biogeogr.* 24, 728–740.
813 <https://doi.org/10.1111/geb.12299>

814 Malamud, B.D., Morein, G., Turcotte, D.L., 1998. Forest Fires: An Example of Self-
815 Organized Critical Behavior. *Science.* 281, 1840 LP – 1842.
816 <https://doi.org/10.1126/science.281.5384.1840>

817 Matthews, T.J., Triantis, K.A., Whittaker, R.J., Guilhaumon, F., 2019. sars: an R package for
818 fitting, evaluating and comparing species–area relationship models. *Ecography.* 42,
819 1446–1455. <https://doi.org/10.1111/ecog.04271>

820 McCarty, J.L., Korontzi, S., Justice, C.O., Loboda, T., 2009. The spatial and temporal
821 distribution of crop residue burning in the contiguous United States. *Sci. Total Environ.*
822 407, 5701–5712. <https://doi.org/10.1016/j.scitotenv.2009.07.009>

823 Mesplé, F., Troussellier, M., Casellas, C., Legendre, P., 1996. Evaluation of simple statistical
824 criteria to qualify a simulation. *Ecol. Modell.* 88, 9–18. <https://doi.org/10.1016/0304->
825 [3800\(95\)00033-X](https://doi.org/10.1016/0304-3800(95)00033-X)

826 Moreno, M.V., Malamud, B.D., Chuvieco, E., 2011. Wildfire frequency-area statistics in
827 Spain. *Procedia Environ. Sci.* 7, 182–187. <https://doi.org/10.1016/j.proenv.2011.07.032>

828 Mouillot, D., Graham, N.A.J., Villéger, S., Mason, N.W.H., Bellwood, D.R., 2013. A functional
829 approach reveals community responses to disturbances. *Trends Ecol. Evol.* 28, 167–
830 177. <https://doi.org/10.1016/j.tree.2012.10.004>

831 Mouillot, F., Schultz, M.G., Yue, C., Cadule, P., Tansey, K., Ciais, P., Chuvieco, E., 2014.
832 Ten years of global burned area products from spaceborne remote sensing-A review:
833 Analysis of user needs and recommendations for future developments. *Int. J. Appl.*

834 Earth Obs. Geoinf. 26, 64–79. <https://doi.org/10.1016/j.jag.2013.05.014>

835 Münkemüller, T., de Bello, F., Meynard, C.N., Gravel, D., Lavergne, S., Mouillot, D.,
836 Mouquet, N., Thuiller, W., 2012. From diversity indices to community assembly
837 processes: a test with simulated data. *Ecography*. 35, 468–480.
838 <https://doi.org/10.1111/j.1600-0587.2011.07259.x>

839 Nogueira, J.M.P.P., Ruffault, J., Chuvieco, E., Mouillot, F., 2017. Can we go beyond burned
840 area in the assessment of global remote sensing products with fire patch metrics?
841 *Remote Sens.* 9. <https://doi.org/10.3390/rs9010007>

842 Oksanen, J., Kindt, R., Pierre, L., O'Hara, B., Simpson, G.L., Solymos, P., Stevens, M.H..
843 H.H., Wagner, H., Blanchet, F.G., Kindt, R., Legendre, P., Minchin, P.R., O'Hara, R.B.,
844 Simpson, G.L., Solymos, P., Stevens, M.H.. H.H., Wagner, H., 2016. *vegan*:
845 *Community Ecology Package*, R package version 2.4-0. R Packag. version 2.2-1.

846 Oom, D., Silva, P.C., Bistinas, I., Pereira, J.M.C., 2016. Highlighting biome-specific
847 sensitivity of fire size distributions to time-gap parameter using a new algorithm for fire
848 event individuation. *Remote Sens.* 8. <https://doi.org/10.3390/rs8080663>

849 Padilla, M., Stehman, S. V., Chuvieco, E., 2014. Validation of the 2008 MODIS-MCD45
850 global burned area product using stratified random sampling. *Remote Sens. Environ.*
851 144, 187–196. <https://doi.org/10.1016/j.rse.2014.01.008>

852 Padilla, M., Stehman, S. V., Ramo, R., Corti, D., Hantson, S., Oliva, P., Alonso-Canas, I.,
853 Bradley, A. V., Tansey, K., Mota, B., Pereira, J.M., Chuvieco, E., 2015. Comparing the
854 accuracies of remote sensing global burned area products using stratified random
855 sampling and estimation. *Remote Sens. Environ.* 160, 114–121.
856 <https://doi.org/10.1016/j.rse.2015.01.005>

857 Pereira, H.M., Ferrier, S., Walters, M., Geller, G.N., Jongman, R.H.G., Scholes, R.J.,
858 Bruford, M.W., Brummitt, N., Butchart, S.H.M., Cardoso, A.C., Coops, N.C., Dulloo, E.,
859 Faith, D.P., Freyhof, J., Gregory, R.D., Heip, C., Höft, R., Hurtt, G., Jetz, W., Karp, D.S.,

860 McGeoch, M.A., Obura, D., Onoda, Y., Pettorelli, N., Reyers, B., Sayre, R.,
861 Scharlemann, J.P.W., Stuart, S.N., Turak, E., Walpole, M., Wegmann, M., 2013.
862 Essential biodiversity variables. *Science*. 339, 277–278.
863 <https://doi.org/10.1126/science.1229931>

864 R Core Team, 2017. R: A language and environment for statistical computing.

865 Rabin, S.S., Melton, J.R., Lasslop, G., Bachelet, D., Forrest, M., Hantson, S., Kaplan, J.O.,
866 Li, F., Mangeon, S., Ward, D.S., Yue, C., Arora, V.K., Hickler, T., Kloster, S., Knorr, W.,
867 Nieradzik, L., Spessa, A., Folberth, G.A., Sheehan, T., Voulgarakis, A., Kelley, D.I.,
868 Colin Prentice, I., Sitch, S., Harrison, S., Arneeth, A., 2017. The Fire Modeling
869 Intercomparison Project (FireMIP), phase 1: Experimental and analytical protocols with
870 detailed model descriptions. *Geosci. Model Dev.* 10, 1175–1197.
871 <https://doi.org/10.5194/gmd-10-1175-2017>

872 Randerson, J.T., Chen, Y., van der Werf, G.R., Rogers, B.M., Morton, D.C., 2012. Global
873 burned area and biomass burning emissions from small fires. *J. Geophys. Res.*
874 *Biogeosciences* 117. <https://doi.org/10.1029/2012JG002128>

875 Ribeiro, P.J.J., Diggle, P.J., 2016. *geoR: Analysis of Geostatistical Data*. R package version
876 1.7-5.2. <https://CRAN.R-project.org/package=geoR>.

877 Rodrigues, J.A., Libonati, R., Pereira, A.A., Nogueira, J.M.P., Santos, F.L.M., Peres, L.F.,
878 Santa Rosa, A., Schroeder, W., Pereira, J.M.C., Giglio, L., Trigo, I.F., Setzer, A.W.,
879 2019. How well do global burned area products represent fire patterns in the Brazilian
880 Savannas biome? An accuracy assessment of the MCD64 collections. *Int. J. Appl.*
881 *Earth Obs. Geoinf.* <https://doi.org/10.1016/j.jag.2019.02.010>

882 Roteta, E., Bastarrika, A., Padilla, M., Storm, T., Chuvieco, E., 2019. Development of a
883 Sentinel-2 burned area algorithm: Generation of a small fire database for sub-Saharan
884 Africa. *Remote Sens. Environ.* 222, 1–17. <https://doi.org/10.1016/j.rse.2018.12.011>

885 Rothermel, R.C.A., 1972. A mathematical model for predicting fire spread in wildland fuels.

886 USDA For. Serv. Res. Pap. INT-115.

887 Short, K.C., 2015. Sources and implications of bias and uncertainty in a century of US
888 wildfire activity data. *Int. J. Wildl. Fire* 24, 883. <https://doi.org/10.1071/WF14190>

889 Short, K.C., 2014. A spatial database of wildfires in the United States, 1992-2011. *Earth*
890 *Syst. Sci. Data* 6, 1–27. <https://doi.org/10.5194/essd-6-1-2014>

891 Sparks, A.M., Boschetti, L., Smith, A.M.S., Tinkham, W.T., Lannom, K.O., Newingham, B.A.,
892 2015. An accuracy assessment of the MTBS burned area product for shrub–steppe
893 fires in the northern Great Basin, United States. *Int. J. Wildl. Fire* 24, 70.
894 <https://doi.org/10.1071/WF14131>

895 Turco, M., Herrera, S., Tourigny, E., Chuvieco, E., Provenzale, A., 2019. A comparison of
896 remotely-sensed and inventory datasets for burned area in Mediterranean Europe. *Int.*
897 *J. Appl. Earth Obs. Geoinf.* 82, 101887. <https://doi.org/10.1016/j.jag.2019.05.020>

898 U.S. Geological Survey, 2017. GeoMAC Wildland Fire Support web page
899 <https://www.geomac.gov/>.

900 van der Werf, G.R., Randerson, J.T., Giglio, L., Collatz, G.J., Mu, M., Kasibhatla, P.S.,
901 Morton, D.C., Defries, R.S., Jin, Y., Van Leeuwen, T.T., 2010. Global fire emissions and
902 the contribution of deforestation, savanna, forest, agricultural, and peat fires (1997-
903 2009). *Atmos. Chem. Phys.* 10, 11707–11735. [https://doi.org/10.5194/acp-10-11707-](https://doi.org/10.5194/acp-10-11707-2010)
904 2010

905 Villéger, S., Grenouillet, G., Brosse, S., 2013. Decomposing functional β -diversity reveals
906 that low functional β -diversity is driven by low functional turnover in European fish
907 assemblages. *Glob. Ecol. Biogeogr.* 22, 671–681. <https://doi.org/10.1111/geb.12021>

908 Villéger, S., Mason, N.W.H., Mouillot, D., 2008. New multidimensional functional diversity
909 indices for a multifaceted framework in functional ecology. *Ecology* 89, 2290–2301.
910 <https://doi.org/10.1890/07-1206.1>

911 Wang, X., Parisien, M.-A., Flannigan, M.D., Parks, S.A., Anderson, K.R., Little, J.M., Taylor,

- 912 S.W., 2014. The potential and realized spread of wildfires across Canada. *Glob. Chang.*
913 *Biol.* 20, 2518–2530. <https://doi.org/10.1111/gcb.12590>
- 914 Warton, D.I., Duursma, R.A., Falster, D.S., Taskinen, S., 2012. smatr 3— an R package for
915 estimation and inference about allometric lines. *Methods Ecol. Evol.* 3, 257–259.
916 <https://doi.org/10.1111/j.2041-210X.2011.00153.x>
- 917 Warton, D.I., Wright, I.J., Falster, D.S., Westoby, M., 2006. Bivariate line-fitting methods for
918 allometry. *Biol. Rev.* 81, 259–291. <https://doi.org/10.1017/S1464793106007007>
- 919
- 920
- 921 Wiegand, T., Uriarte, M., Kraft, N.J.B., Shen, G., Wang, X., He, F., 2017. Spatially Explicit
922 Metrics of Species Diversity, Functional Diversity, and Phylogenetic Diversity: Insights
923 into Plant Community Assembly Processes. *Annu. Rev. Ecol. Evol. Syst.* 48, 329–351.
924 <https://doi.org/10.1146/annurev-ecolsys-110316-022936>
- 925 WMO, 2016. The Global Observing System for Climate: Implementation Needs 200, 325.
- 926 Yue, C., Ciais, P., Cadule, P., Thonicke, K., Archibald, S., Poulter, B., Hao, W.M., Hantson,
927 S., Mouillot, F., Friedlingstein, P., Maignan, F., Viovy, N., 2014. Modelling the role of
928 fires in the terrestrial carbon balance by incorporating SPITFIRE into the global
929 vegetation model ORCHIDEE - Part 1: Simulating historical global burned area and fire
930 regimes. *Geosci. Model Dev.* 7, 2747–2767. <https://doi.org/10.5194/gmd-7-2747-2014>
- 931 Zhu, L., Fu, B., Zhu, H., Wang, C., Jiao, L., Zhou, J., 2017. Trait choice profoundly affected
932 the ecological conclusions drawn from functional diversity measures. *Sci. Rep.* 7, 3643.
933 <https://doi.org/10.1038/s41598-017-03812-8>

934 **List of Figure Captions**

935 **Fig. 1:** Theoretical functional diversity trait-based approach adapted from Mouillot et al.
936 (2013) and Villéger et al. (2013, 2008) to assess satellite-derived fire patches in four steps.
937 Functional trait (F_{trait}) is a morphological feature of the fire patch. Functional diversity indices

938 (FDIs) include functional fire-patch number (F_{fp}), functional richness (F_{ric}) and functional
939 dispersion (F_{dis}). Continental scale tile-to-tile Standardized Major Axis (SMA) regression of
940 FDIs, and tile-level functional beta diversity (F_{β}), functional turnover (F_{turn}) and functional
941 nestedness (F_{nest}) were used in the assessment. For a simple graphical display, the first step
942 shows tiles from only one product and the reference data. Similarly, the second step shows
943 the fire patches present in a functional space of only two traits in one tile, and the fourth step
944 shows functional spaces as a circle. A Venn diagram illustrates these cases.

945 **Fig. 2.** Relationships of functional diversity indices between the FRY v1.0 FireCCI41 product
946 and the reference data. Each point is a 2° tile containing multiple patches. Left column refers
947 to the number of fire patches (F_{fp}), middle column to functional richness (F_{ric}) and the right
948 column to functional dispersion (F_{dis}). The squared correlation coefficient (r^2) is provided. In
949 addition, for every significant r^2 ($p < 0.05$), the Standardized major axis (SMA) lines, SMA
950 slope (b), SMA intercept (a), and confidence intervals at the 95% level (95% CI) are
951 provided. Different colours identify data across tiles (n) in North America (NA) Boreal North
952 America (BONA) and Temperate North America (TENA). The horizontal-axis presents the
953 functional diversity index in the reference data and the vertical-axis in the FRY-FireCCI41
954 cut-off values. Both axes are in log10-scale for F_{fp} and F_{dis} .

955 **Fig. 3.** Relationships of functional diversity indices between the FRY v1.0 MCD64A1 product
956 and the reference data. Each point is a 2° tile containing multiple patches. Left column refers
957 to the number of fire patches (F_{fp}), middle column to functional richness (F_{ric}) and the right
958 column to functional dispersion (F_{dis}). The squared correlation coefficient (r^2) is provided. In
959 addition, for every significant r^2 ($p < 0.05$), the Standardized major axis (SMA) lines, SMA
960 slope (b), SMA intercept (a), and confidence intervals at the 95% level (95% CI) are
961 provided. Different colours identify data across tiles (n) in North America (NA), Boreal North
962 America (BONA) and Temperate North America (TENA). The horizontal axis presents the

963 functional diversity index in the reference data and the vertical axis in the FRY-MCD64A1
964 cut-off values. Both axes are in log10-scale for F_{fp} and F_{dis} .

965 **Fig. 4.** Functional dissimilarities within tiles between the FRY v1.0 FireCCI41 product and
966 the reference data in North America (NA), Boreal North America (BONA) and Temperate
967 North America (TENA). Functional beta diversity (F_{β}) is the sum of turnover (F_{turn}) and
968 nestedness (F_{nest}) as explained in the text. Means across cut-off values with the same letter
969 and means within cut-off values with the same number are not significantly different ($p <$
970 0.05).

971 **Fig. 5.** Examples of functional dissimilarities within tiles between FRY v1.0 FireCCI41 (blue
972 volume) and the reference data (green volume) in California (Tile 34N, -120W), Florida (Tile
973 26N, -82W) and Quebec (Tile 50N, -72W) for specific traits considered: size, direction,
974 elongation of patches.

975 **Fig. 6.** Functional dissimilarities within tiles between the FRY v1.0 MCD64A1 product and
976 the reference data in North America (NA), Boreal North America (BONA) and Temperate
977 North America (TENA). Functional beta diversity (F_{β}) is the sum of turnover (F_{turn}) and
978 nestedness (F_{nest}) as explained in the text. Means across cut-off values with the same letter
979 and means within cut-off values with the same number are not significantly different ($p <$
980 0.05).

981 **Fig. 7.** Examples of functional dissimilarities within tiles between FRY v1.0 MCD64A1 (red
982 volume) and the reference data (green volume) in California (Tile 34N, -120W), Florida (Tile
983 26N, -82W) and Quebec (Tile 50N, -72W) for specific traits considered: size, direction,
984 elongation of patches.

985

986 **List of Figure Captions in Supplementary Data**

987 **Fig. S1.** Functional diversity indices in the FRY v1.0 FireCCI41 product in North America.
988 Functional fire patches (F_{fp}), functional richness (F_{ric}) and functional dispersion (F_{dis}).

989 **Fig. S2.** Functional diversity indices in the FRY v1.0 FireCCI41 product in California (Tile
990 34N, -120W). Functional fire patches (F_{fp}), functional richness (F_{ric}) and functional dispersion
991 (F_{dis}).

992 **Fig. S3.** Functional diversity indices in the FRY v1.0 FireCCI41 product in Florida (Tile 26N,
993 -82W). Functional fire patches (F_{fp}), functional richness (F_{ric}) and functional dispersion (F_{dis}).

994 **Fig. S4.** Functional diversity indices in the FRY v1.0 FireCCI41 product in Quebec (Tile 50N,
995 -72W). Functional fire patches (F_{fp}), functional richness (F_{ric}) and functional dispersion (F_{dis}).

996 **Table S1.** Statistical summary of functional diversity indices (FDIs) in the FRY v1.0
997 FireCCI41 product across North America (NA), Boreal North America (BONA) and
998 Temperate North America (TENA). Functional fire patches (F_{fp}), functional richness (F_{ric}) and
999 functional dispersion (F_{dis}).

1000 **Fig. S5.** Functional diversity indices in the FRY v1.0 MCD64A1 product in North America
1001 (mainland United State and Canada). Functional fire patches (F_{fp}), functional richness (F_{ric})
1002 and functional dispersion (F_{dis}).

1003 **Fig. S6.** Functional diversity indices in the FRY v1.0 MCD64A1 product in California (Tile
1004 34N, -120W). Functional fire patches (F_{fp}), functional richness (F_{ric}) and functional dispersion
1005 (F_{dis}).

1006 **Fig. S7.** Functional diversity indices in the FRY v1.0 MCD64A1 product in Florida (Tile 26N,
1007 -82W). Functional fire patches (F_{fp}), functional richness (F_{ric}) and functional dispersion (F_{dis}).

1008 **Fig. S8.** Functional diversity indices in the FRY v1.0 MCD64A1 product in Quebec (Tile 50N,
1009 -72W). Functional fire patches (F_{fp}), functional richness (F_{ric}) and functional dispersion (F_{dis}).

1010 **Table S2.** Statistical summary of functional diversity indices (FDIs) in the FRY v1.0
1011 MCD64A1 product in North America (NA), Boreal North America (BONA) and Temperate
1012 North America (TENA). Functional fire patches (F_{fp}), functional richness (F_{ric}) and functional
1013 dispersion (F_{dis}).

1014 **Fig. S9.** Functional diversity indices in the reference data at two spatial resolutions (i.e., 300
1015 m and 500 m) in North America (mainland United State and Canada). Functional fire
1016 patches (F_{fp}), functional richness (F_{ric}) and functional dispersion (F_{dis}).

1017 **Fig. S10.** Functional diversity indices in the reference data at two spatial resolutions (i.e.,
1018 300 m and 500 m) in California (Tile 34N, -120W). Functional fire patches (F_{fp}), functional
1019 richness (F_{ric}) and functional dispersion (F_{dis}).

1020 **Fig. S11.** Functional diversity indices in the reference data at two spatial resolutions (i.e.,
1021 300 m and 500 m) in Florida (Tile 26N, -82W). Functional fire patches (F_{fp}), functional
1022 richness (F_{ric}) and functional dispersion (F_{dis}).

1023 **Fig. S12.** Functional diversity indices in the reference data at two spatial resolutions (i.e.,
1024 300 m and 500 m) in Quebec (Tile 50N, -72W). Functional fire patches (F_{fp}), functional
1025 richness (F_{ric}) and functional dispersion (F_{dis}).

1026 **Table S3.** Statistical summary of functional diversity indices (FDIs) in the reference data at
1027 two spatial resolutions (i.e., 300 m and 500 m) in North America (NA), Boreal North America
1028 (BONA) and Temperate North America (TENA). Functional fire patches (F_{fp}), functional
1029 richness (F_{ric}) and functional dispersion (F_{dis}).

1030 **Table S4.** Statistical summary of functional dissimilarities between the FRY v1.0 products
1031 and the reference data at two spatial resolutions (i.e., 300 m and 500 m) in North America
1032 (NA), Boreal North America (BONA) and Temperate North America (TENA). Functional beta
1033 diversity (F_{beta}) and its two components of turnover (F_{turn}) and nestedness (F_{nest}).

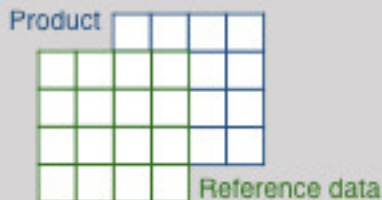
1034 **Fig. S13.** Frequency density of fire-patch size in the FRY v1.0 FireCCI41 product (blue
1035 points) and reference data at 300 m resolution (green points) across North America (NA),
1036 Boreal North America (BONA) and Temperate North America (TENA). The frequency
1037 density of fire-patch size was calculated as in Moreno et al. (2011).

1038 **Fig. S14.** Frequency density of fire-patch size in the FRY v1.0 MCD64A1 product (red
1039 points) and reference data at 500 m resolution (green points) across North America (NA),
1040 Boreal North America (BONA) and Temperate North America (TENA). The frequency
1041 density of fire-patch size was calculated as in Moreno et al. (2011).

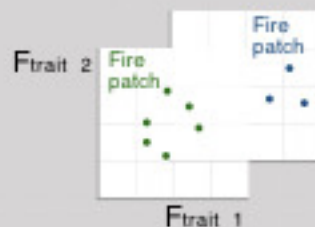
1042 **Fig. S15.** Burned area (ha) per tile (n) in the FRY v1.0 FireCCI41 product and reference
1043 data at 300 m resolution across North America (NA), Boreal North America (BONA) and
1044 Temperate North America (TENA).

1045 **Fig. S16.** Burned area (ha) per tile (n) in the FRY v1.0 MCD64A1 product and reference
1046 data at 500 m resolution across North America (NA), Boreal North America (BONA) and
1047 Temperate North America (TENA).

First step: sample the fire-patch products

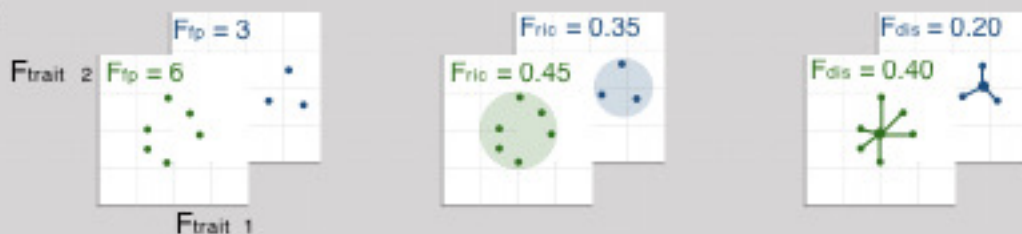


Second step: build the functional space

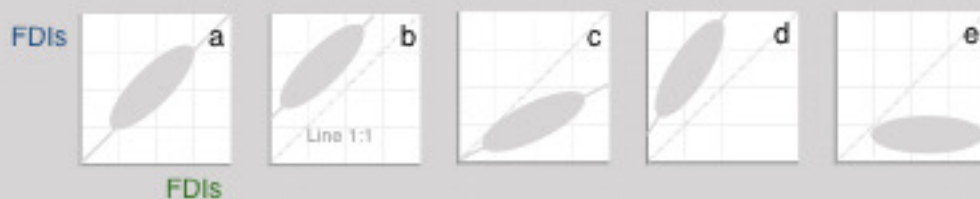


Third step: assessment of the functional structure

FDIs



SMA regression



Fourth step: assessment of the functional dissimilarity

